Dynamics and transport of sulfur dioxide over the Yellow Sea during TRACE-P

Fang Huang Tu, Donald C. Thornton, Alan R. Bandy, and Mi-Sug Kim

Department of Chemistry, Drexel University, Philadelphia, Pennsylvania, USA

Gregory Carmichael and Youhua Tang

Center for Global and Regional Environmental Research, University of Iowa, Iowa City, Iowa, USA

Lee Thornhill and Glenn Sachse

NASA Langley Research Center, Hampton, Virginia, USA

[1]   Fast time resolution (>1 Hz) sulfur dioxide (SO_2) measurements were obtained using an atmospheric pressure ionization mass spectrometer with isotopically labeled internal standard on the NASA Wallops P-3B during the NASA Transport and Chemical Evolution Over the Pacific (TRACE-P) field experiment. The high time resolution for SO_2 allowed a view into the dynamics of SO_2 transport, including the effects of clouds. Two missions along 124.5°E from the vicinity of Taiwan to the northern Yellow Sea near the Korean peninsula were flown on consecutive days with quite different weather conditions. Although the winds on both flights were westerly to northwesterly, the SO_2 concentrations were markedly different in vertical and horizontal distributions. Together with turbulence measurements and other high rate data on the P-3B, we have assessed how cloud processing and atmospheric dynamics may have caused the differences in the SO_2 distributions. Below 2 km, SO_2 layers of a few hundred meters depth were often isolated from the mixed layer. The relatively slow process of entrainment limited loss of SO_2 to the marine mixed layer. When compared to 3-D model results of SO_2 along the flight track, the in situ SO_2 data showed that the model poorly represented the SO_2 distribution along the flight track for the cloudy day, while the model gave a reasonably good representation of the in situ data during the clear air flight. On the clear air flight day, the model achieved a closer representation of the SO_2 distribution, but it overestimated the SO_2 concentrations just above the well-mixed boundary layer. The deviations between the observations and the model appear to be related the treatment of the boundary layer dynamics.   *INDEX TERMS:* 0322 Atmospheric Composition and Structure: Constituent sources and sinks; 0345 Atmospheric Composition and Structure: Pollution—urban and regional (0305); 0365 Atmospheric Composition and Structure: Troposphere—composition and chemistry; 0368 Atmospheric Composition and Structure: Troposphere—constituent transport and chemistry; *KEYWORDS:* sulfur dioxide, transport, dynamics, TRACE-P, Pacific

1.   Introduction

[2]   The high level of economic development in east Asia during the past two decades has relied on fossil fuels for energy production, in particular, on high sulfur content coal. Sulfur dioxide (SO_2) emissions peaked in 1996 in the major source regions of East Asia, but the total emissions of SO_2 are still very large [*Streets et al.*, 2003]. The NASA Global Troposphere Experiment (GTE) Transport and Chemical Evolution over the Pacific (TRACE-P) mission was designed to study the transport and evolution of anthropogenic chem-ical species and their impact on the north Pacific troposphere [*Jacob et al.*, 2003]. The TRACE-P mission employed a wider suite of measurements than in past GTE missions and a wide variety of predictive chemical and meteorlogical models than earlier field programs in this region.

[3]   Sulfur dioxide plays a very important role in atmospheric sulfur cycle through its role in the formation of new aerosol and the modification of existing aerosol. The major sources of SO_2 are from anthropogenic fuel combustion and from volcanoes. The reliance of East Asian nations on fossil fuels in their rapid development over the last two decades has lead to concern about the potential impact of SO_2 on the western Pacific troposphere. There is also the concern about

the impact on global climate through the formation and modification of aerosols and their effects on the radiation balance of the atmosphere. Assessing the relative contributions of anthropogenic and volcanic sources can be done through estimates of the anthropogenic emissions and the flux of SO$_2$ from volcano emissions. Neither of these estimates is easy to determine precisely because the large area over which the anthropogenic sources are dispersed and the remoteness and difficulty in measuring the SO$_2$ fluxes from volcanoes.

[4]   The NASA Pacific Exploratory Missions West (PEM West) studied the western Pacific region in September 1991 (phase A) [*Hoell et al.*, 1996] and in February–March 1994 (phase B) [*Hoell et al.*, 1997]. The anthropogenic SO$_2$ measurements from these earlier missions [*Thornton et al.*, 1996, 1997] have clearly shown the impact on the northern Pacific when compared to the central and southern Pacific [*Thornton et al.*, 1999]. Volcanic sources of SO$_2$ have also been a significant source of SO$_2$ to the Pacific troposphere, and they remain a significant source in this region, particularly around Japan (E. Venzke et al., Global volcanism, 1968 to the present, Smithsonian Institution, Global Volcanism Program Digital Information Service, GVP-4, 2002, available at http://www.volcano.si.edu/gvp/reports/). Transport of 0.1–2 ppbv of SO$_2$ over the Yellow Sea in mid to late April has been observed to be variable between the surface and 3 km with the highest concentrations below 1 km [*Kim et al.*, 2001]. How SO$_2$ is transported from its sources and how SO$_2$ impacts the western Pacific troposphere are very important issues that are not fully resolved.

[5]   During the TRACE-P mission, the fast time resolution (>1Hz) SO$_2$ data allowed a view of the dynamics of SO$_2$ transport. This high time resolution allowed the study of small spatial scale features of SO$_2$ in and around clouds, in ship plumes, and the vertical profile in plumes. With the turbulent air motion measurement system (TAMMS) [*Thornhill et al.*, 2003] on the NASA Wallops Flight Facility P-3B, we were able to study the details of the vertical distribution of SO$_2$ in the lower troposphere and in the marine mixed layer on the timescales of the atmospheric turbulence. The results of the TRACE-P experiment will shed new light on the role of atmospheric dynamics in controlling the distribution of SO$_2$. As a consequence we can better understand how long range transport of SO$_2$ occurs over the northern Pacific.

2.   Experiment

[6]   On the TRACE-P mission, the SO$_2$ measurements on the NASA Wallops P-3B were obtained by atmospheric pressure ionization mass spectrometry using an isotopically labeled internal standard (APIMS/ILS). The details of the quadrupole APIMS/ILS system with a ^{63}Ni ion source have been described recently [*Thornton et al.*, 2002a]. In short, the technique involves continuously adding ^{34}SO$_2$ as an internal standard to ambient air as it is drawn into the aircraft through a Teflon lined inlet through the aircraft wall [*Bandy et al.*, 1993]. The ion chemistry and declustering region produced SO$_5^-$ ions, which were monitored alternately at m/e 112 for the ambient signal and m/e 114 for the internal isotopically labeled standard. Each ion signal count was integrated for 20 ms and the ambient SO$_2$ concentration was computed for every 40 ms (25 Hz sampling rate) after taking into account the isotopic abundances as described previously [*Bandy et al.*, 1993]. A correction was also made for background ion signals determined from SO$_2$ free air (Scott-Marrin, Inc, Riverside, California) and from ambient air without the standard added [*Thornton et al.*, 2002a].

[7]   The TRACE-P data archive contains a 1-s integral of 25 Hz data. The lower limit of detection for 10-s integration is 1 pptv. The precision is estimated to be 3 pptv for a 1-s integration for SO$_2$ concentrations below 100 pptv and <2% above 100 pptv. Accuracy of the measurements is estimated to be 5% based on calibration of the 153 ppbv ^{34}SO$_2$ in ultrapure nitrogen cylinder (Scott-Marrin, Inc., Riverside, California) using three ^{32}SO$_2$ permeation tubes (VICI Metronics, Poulsbo, Washington), which were gravimetrically calibrated.

[8]   The TAMMS provided 25 Hz data for the u, v, w components of the wind, water vapor mixing ratio (MR) from a Lyman α absorption sensor, static temperature, and pressure [*Thornhill et al.*, 2003]. The SO$_2$ count data were recorded by the TAMMS data system to insure that the time recorded for the SO$_2$ counts would be identical to the time recorded for the three component wind data. Additional meteorological data were provided by the GTE project for the P-3B (TRACE-P data archive).

[9]   Five-day backward trajectories (http://www-gte.larc. nasa.gov/trace/TP_dat.htm) were calculated using a kinematic model, i.e., employing the u, v, and w wind components from the ECMWF analyses [*Fuelberg et al.*, 2003]. A cubic spline procedure was used to vertically interpolate the gridded data from the 61 initial sigma levels to 191 constant pressure levels at 5-hPa intervals between 1000 and 50 hPa. Linear interpolation provided values within these 5-hPa intervals and at the parcel's precise horizontal locations. Linear interpolation also was used to temporally interpolate at 5-min time steps. Additional details about the trajectory model, along with a comparison between kinematic and isentropic trajectories, are given by *Fuelberg et al.* [1996].

3.   Results

[10]   One of the major goals of TRACE-P was to understand the processes that control the transport and evolution of chemical species in the Pacific troposphere. Predictive and interpretive chemical transport models are useful tools for understanding the large scale of the transport and the chemical processing that occurs over the Pacific because of the difficulty of obtaining data on a regular basis. The large-scale view depends on a myriad of processes that descend into smaller and smaller scales down to the order of molecular processes. The capability of the model output in representing actual conditions as indicated by observations depends on the quality of the estimates of the chemical inputs and the validity of the parameterizations that must be used to account for the small-scale chemical and physical processes that cannot be easily represented in fine detail or where the details of the process are not completely known.

[11]   The availability of high time and spatial resolution data provides a broader base on which to evaluate model output. This more detailed database also provides an input of information with which to refine the model process
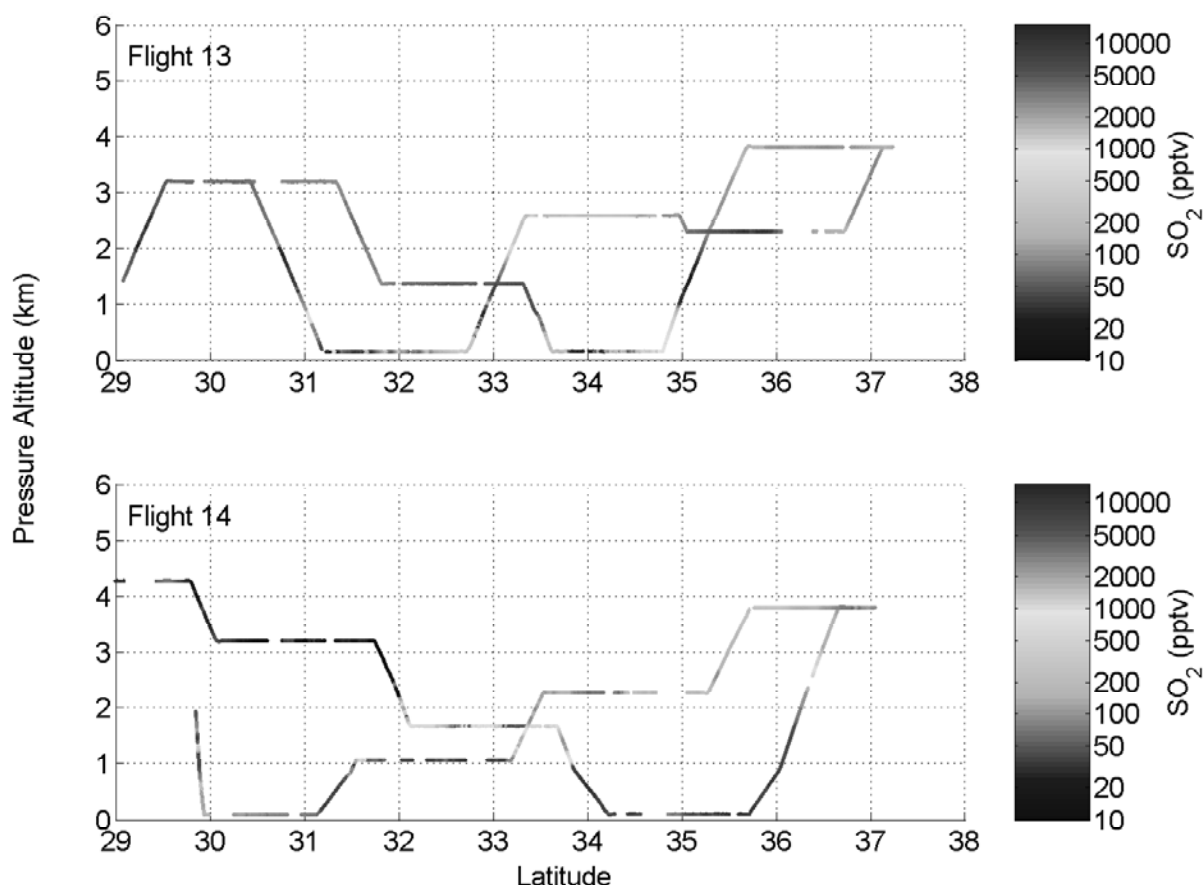
Figure 1. Sulfur dioxide distributions along the 124.5°E flight path for TRACE-P P-3B flight 13 during frontal passage and flight 14 behind the front. The profile just south of 30°N for flight 14 as the aircraft turned east from the 124.5°E track illustrates the downwind advection of SO₂. See color version of this figure at back of this issue.

parameterizations. Most transport models have very good representation of the meteorological processes that occur over small and large scales because of the volume of data that is available. The representation of chemical processes also can provide good representations of the chemical field for homogeneous gas phase chemistry. The primary uncertainties with chemical transport models appear to be on the links between the physical and chemical processes [*Chin et al.*, 2000; *Carmichael et al.*, 2002]. The uncertainties can include the interaction between the source emissions and the atmosphere, heterogeneous processing of chemical constituents, and the mixing of air masses from widely different sources.

[12] The high time and spatial resolution for SO_2 on the P-3B clearly showed that the vertical distribution of SO_2 was often confined to layers of 200 to 300 m deep. In addition, there were often shallow mixed layers with two layers below the boundary layer top marked by the temperature inversion. We have investigated these layers using the turbulence data, thermodynamic data, and other chemical tracers to understand the SO_2 distribution in these layers. One driving force for this study was to characterize these layers because they may be responsible for the transport of SO_2 to the central Pacific troposphere at altitudes below 4

km but above the mixed layer. *Cho et al.* [2003] have characterized the turbulence and stability of the free troposphere from the TRACE-P TAMMS data. Their analyses supported the idea that differential advection can maintain tracer gradients in the free troposphere. The transport occurred in layers that are bounded by thin turbulent layers, which maintain their integrity over significant distances.

3.1. Yellow Sea P-3B Missions

[13] During TRACE-P the flight plans for the P-3B for 17–18 March 2001 were to execute a stair step pattern along 124.5°E extending from 25°N north of Taiwan into Yellow Sea as far as 37°N. The chemical transport models predicted outflow from China north of 25°N at altitudes from 1.3 to 4 km. The SO_2 distributions observed during these two flights along their common flight track from 29°N to 38°N have been analyzed in the context of the meteorological conditions to illustrate how the dynamics were affecting the SO_2 distributions. The observations were also compared to the CFORS/STEM-2K1 chemical transport model results for the same period.

[14] On 17 March 2001 flight 13 of the P-3B originated in Hong Kong and executed its flight plan along 124.5°E to the Yellow Sea and terminated at Kadena, Okinawa
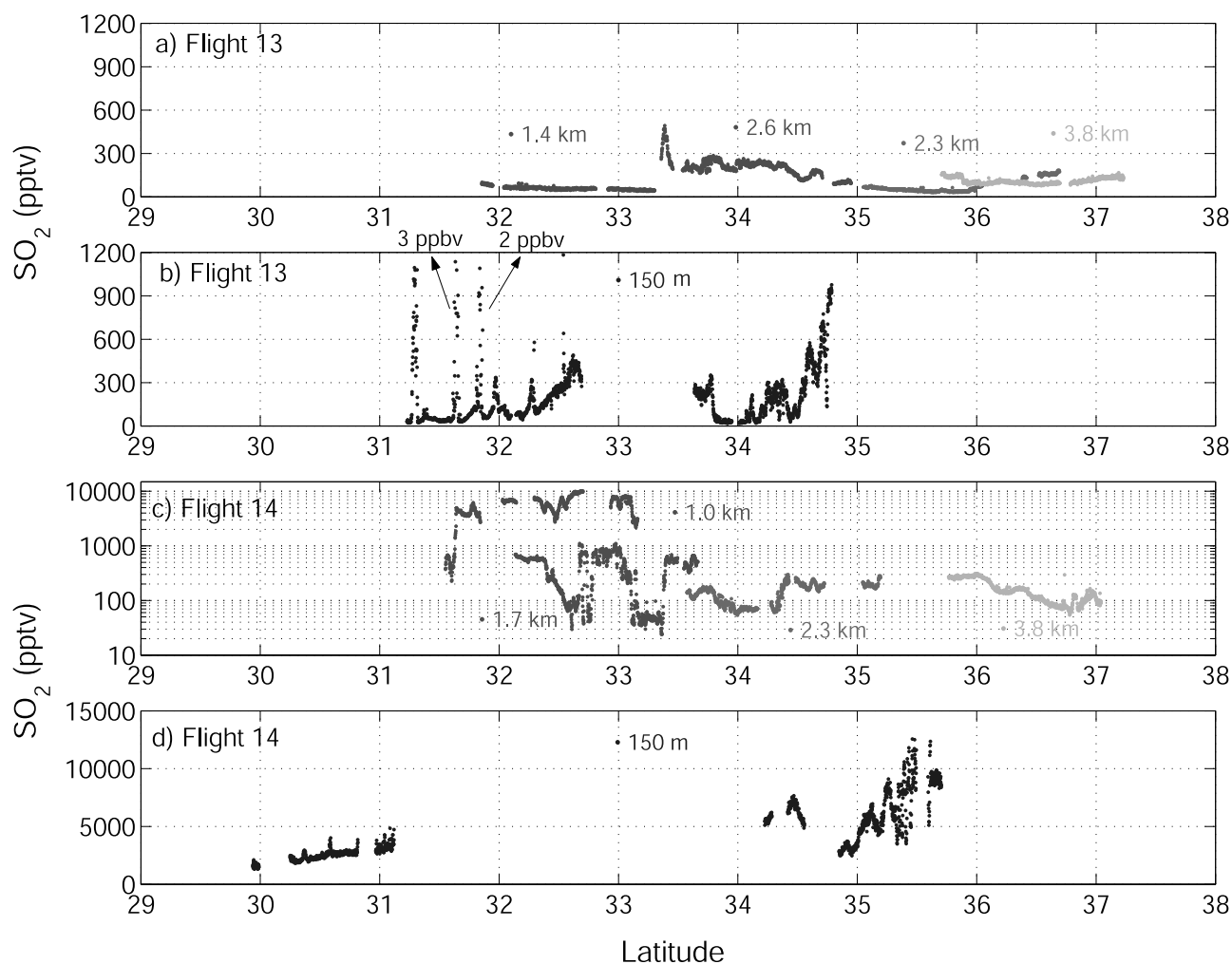
Figure 2. Sulfur dioxide distribution along 124.5°E for the level legs for flights 13 and 14. (a) and (c) above the mixed layer, (b) in mixed layer with spikes of SO$_2$ to 3 ppbv from ship plumes from 31.2°N to 32.5°N, (d) in the mixed layer for 30–31°N and in and out of the mixed layer between 34°N and 36°N. See color version of this figure at back of this issue.

(127.75°E 26.38°N). On 18 March 2001 flight 14 of the P-3B was flown along 124.5°E from the East China Sea north of Taiwan to the Yellow Sea near the Korean peninsula. The SO$_2$ distribution along the 124.5°E meridian is shown in Figure 1. A small portion of the vertical profile at 30°N for flight 14 is shown in Figure 1 to illustrate the downwind extent of the SO$_2$ advection east of 124.5°E. At the end of the 150 m leg along 124.5°E, the aircraft then turned east along 29.6°N until it could proceed along the east coast of Japan where the flight terminated at Yokota Air Base (139.35°E 35.7°N).

[15] In the region where these two flights took place weather conditions were quite different. A front passed through the area on 16–17 March 2001 with clear air filling in over the Yellow Sea on 18 March 2001. The precipitation analysis daily images for 15–18 March 2001 from the Tropical Rainfall Measurement Mission (TRMM) micro-wave imager (TMI) (Global Precipitation Climatology Project, Laboratory for Atmospheres, NASA Goddard Space Flight Center, http://precip.gsfc.nasa.gov/rain_pages/daily_ choice.html) indicated a wide area of 0.5–1 cm/d

of rain from 26°N to 32°N on 16 March 2001. The Special Sensor Microwave Imager (SSM/I) on the Defense Meteorological Satellite program (DMSP) for 16 March 2001 showed the same wide area of rain but the heaviest rain (8 cm/d) was centered on 125°E, 30°N. The three hour images from the GMS-5 infrared channels tuned to the micro-wave imaging rainfall data by the Naval Research Laboratory (http://asd-www.larc.nasa.gov/David/gtewestpacprecip.html) showed that there was a band of 1–2 cm of rain along 34°N and with the maximum near on 125°E at 0300 UTC on 16 March 2001. There was no rainfall in the study area indicated by any satellite data for the two flight days.

[16] On 17 March 2001 the aircraft intercepted several low-level stratus layers off the coast of China along the 124.5°E meridian. Above the P-3B flight path on 17 March 2001 there also were some high altitude clouds between 33°N to 38°N. On 18 March 2001, the study area was clear of clouds since the front had passed through the previous evening. (Satellite and weather summaries are available on the GTE archive website http://asd-www.larc.nasa.gov/David/gtetracepp3bwxpg.html.)
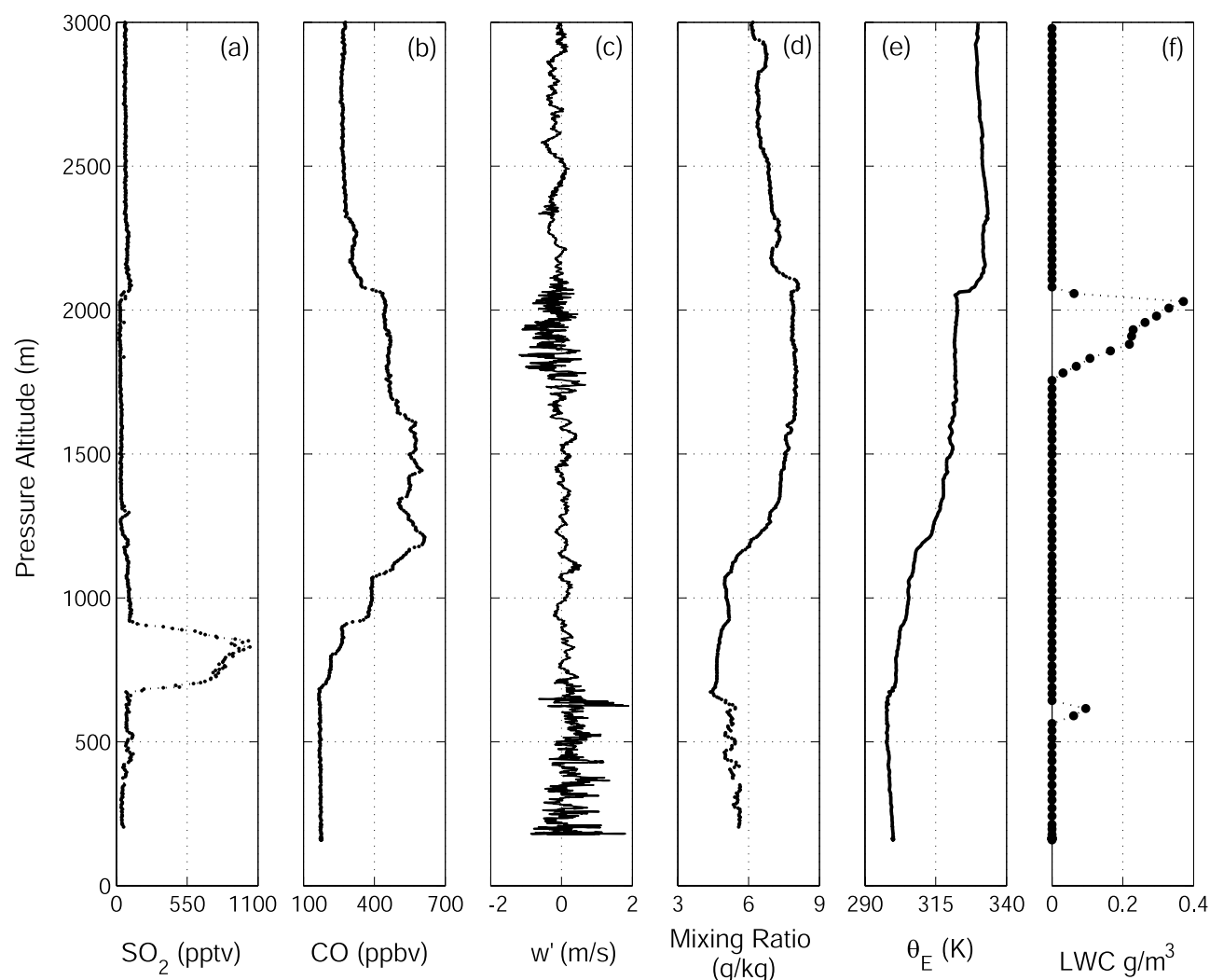
Figure 3. Vertical ascent profiles of (a) SO_2, (b) CO, (c) w' (the vertical wind component about the mean vertical wind for the profile shown), (d) water vapor mixing ratio (MR), (e) equivalent potential temperature (θ_e), and (f) liquid water content (LWC) near 124.5°E, 31.2°N for flight 13. Data are 1 Hz except for 10 Hz w' and 0.2 Hz LWC. SO_2 plume is above the mixed layer top at 650 m, which is indicated by where the large variance in w' decreases. Cloud is indicated by the LWC at 600 m and 2 km.

[17] Although the winds on both flights were from the west to northwest, the SO_2 concentrations were markedly different in vertical and horizontal distributions along 124.5°E (Figure 1). The SO_2 concentrations along 124.5°E for both flights increased from south to north as predicted by the transport models. The highest SO_2 concentrations on each flight were below 2 km with the peak SO_2 levels at or below 1 km. However, this view of the distribution (Figure 1) does not indicate the high spatial and temporal variation of the SO_2 concentrations in these flight profiles.

[18] The SO_2 concentrations for the level flight legs between the surface and 3.8 km for the flight track along 124.5°E are shown in Figure 2. The northern end of the track was within 160 km of the middle of the Korean peninsula, and near the southern end of flight track at 30°N Shanghai was 300 km to the west. Flight 13 had concentrations about an order of magnitude lower than flight 14 below 2 km. Above 3 km both flights had SO_2

concentrations <150 pptv that appeared to have been transported from much further west than coastal China. These upper air masses were likely isolated from the air mass below as shown in the thermodynamic structure and the vertical velocity profiles in the following sections.

3.2. Flight 13

[19] Along the 124.5°E track on flight 13, the winds for the 150 m level legs were 300° to 320° while the winds for the 1.4 km and 2.6 km levels were 260° to 270°. At 150 m there appeared to be two plumes: one north of 34°N and another between 32°N and 33.8°N (Figure 2b). Between these plumes near 34°N the SO_2 concentrations were 30–40 pptv, which was typical of remote North Pacific air [*Thornton et al.*, 1999]. This decrease in SO_2 at 150 m between 33.8°N and 34°N was likely the result of rainout and washout in the rainband described above in the tuned GMS-5 satellite image. The SO_2 concentrations of 40–70 pptv at 1.4 km between 32°N and 33.3°N and may have
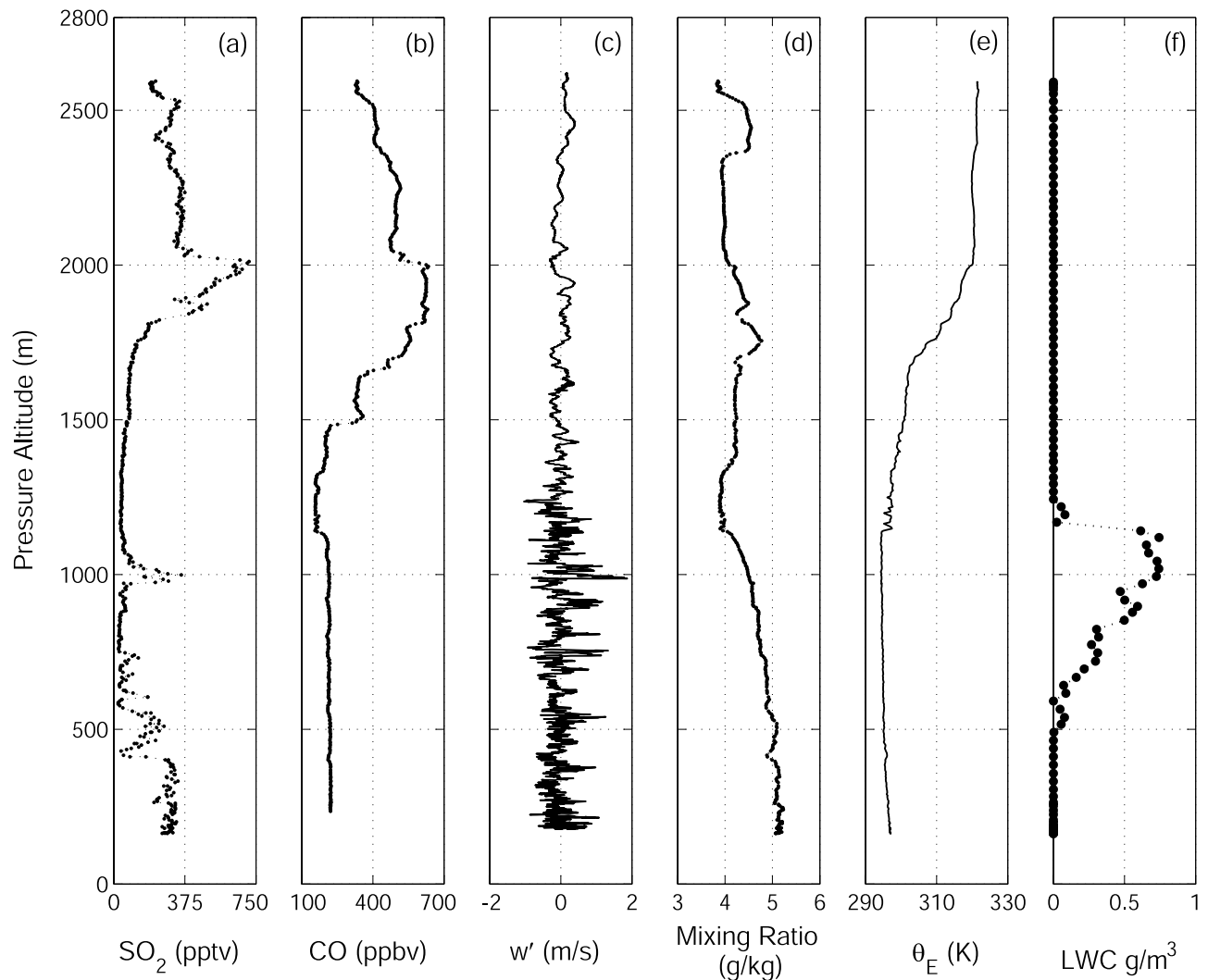
Figure 4. Vertical descent profiles of (a) SO_2, (b) CO, (c) w' (the vertical wind component about the mean vertical wind for the profile shown), (d) water vapor mixing ratio (MR), (e) equivalent potential temperature (θ_e), and (f) liquid water content (LWC) near 124.5°E, 32.7°N for flight 13. Data are 1 Hz except for 10 Hz w' and 0.2 Hz LWC. Note the largest SO_2 concentrations between 0.5 and 1 km that corresponded to positive excursions in w', and at 1 km the SO_2 concentration was the same as below 400 m.

been reduced by cloud processing or rain. At 2.6 km the SO_2 levels were 200–300 pptv (Figure 2a), which was comparable to the mixed layer concentrations at 33.7°N and 34.4°N. The SO_2 at 2.6 km may have been above the clouds and apparently was not as affected by rainout or washout that removed SO_2 around 34°N in the mixed layer below.

[20] At 150 m between 31°N and 33°N for flight 13, fresh ship plumes were a major local source of the SO_2 (Figure 2b). The three largest SO_2 ship plumes were very fresh as there were decreases in ozone (O_3) (M. Avery, TRACE-P data archive) as well as ppbv levels of nitric oxide (NO) (Y. Kondo, TRACE-P data archive). An estimate of the impact of the ship plumes was made by integrating only the short period spikes in SO_2 from the ship plumes compared to the integral SO_2 concentration along this leg assuming a constant mixed layer height. By this estimate the ship plumes would account for 46% of the SO_2 along this leg. However, the mixed layer height changed from 650 m at 31.2°N (Figure 3c) to 1.2 km at

32.7°N (Figure 4c) with a cloud base of 500 m. Without knowing how extensive this cloud was along the track, it is difficult to estimate the true impact of the ship plumes for this leg. On the basis of these data it appears that ship plumes can have a significant impact on the mixed layer when SO_2 transported from the continent is greatly reduced by precipitation [*Streets et al.*, 2000].

[21] In contrast to the southern mixed layer leg, the northern leg over the Yellow Sea (33.6°N to 34.8°N) did not appear to have any fresh ship plumes based on the NO and O_3 data. The decreases in SO_2 at the northern end were associated with high relative humidity implying that the SO_2 may have been removed by washout or by cloud processing. For example, near 34.7°N SO_2 dropped from 700 pptv to 100 pptv, which was coincident with high relative humidity. The detection of droplets on the Gerber particle volume measurement (PVM) probe (A. Clarke, TRACE-P data archive) indicated that there might have been drizzle in this region.
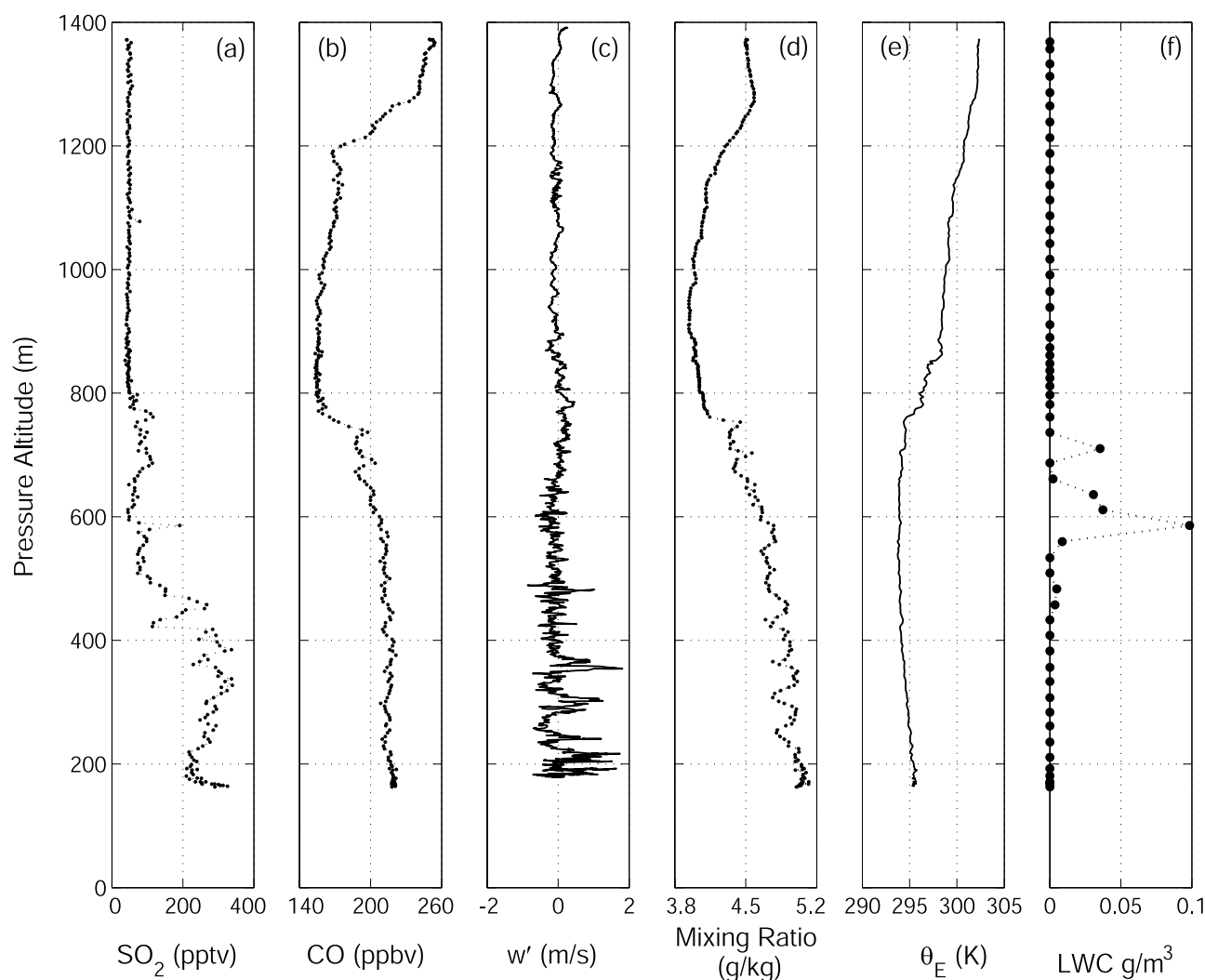
Figure 5. Vertical descent profiles of (a) SO₂, (b) CO, (c) w' (the vertical wind component about the mean vertical wind for the profile shown), (d) water vapor mixing ratio (MR), (e) equivalent potential temperature (θ_e), and (f) liquid water content (LWC) near 124.5°E, 33.6°N for flight 13. Data are 1 Hz except for 10 Hz w' and 0.2 Hz LWC. SO₂ appeared to have been lost to heterogeneous processes in cloud above 500 m. Drier, less turbulent air with lower CO was above cloud top at 700 m and appeared to be diluting the moister CO-richer air below causing the cloud to dissipate (see back trajectory with circles in Figure 7).

[22] The vertical profiles that bracket the mixed layer legs of flight 13 (Figure 2b) illustrate the highly structured layers in the SO₂ vertical distribution (Figures 3a, 4a, 5a, and 6a). The most striking feature of these vertical profiles is the layering of SO₂. The key to understanding this layered structure lies in the turbulence structure, which can be observed from the variance of the vertical wind component from the TAMMS data [*Thornhill et al.*, 2003]. The vertical profiles of w' ($w' = w_i - w_{mean}$) (Figures 3c, 4c, 5c, and 6c) more clearly delineate the mixed layers than the vertical profiles of water vapor mixing ratio (Figures 3d, 4d, 5d, and 6d) or equivalent potential temperature (θ_e) (Figures 3e, 4e, 5e, and 6e) The well-mixed part of the boundary layer is indicated by the large variance in w', which reflects the large range in eddy scales that existed. When the variance is very small there is, in effect, a very low rate of vertical or horizontal mixing. The variance in w' is also useful in

determining if the boundary layer consisted of a well mixed lower layer and an intermittently mixed upper layer [*Russell et al.*, 1998; *Wang et al.*, 1999]. The liquid water content (LWC) derived from the PVM probe clearly marked the presence of the cloud layers for flight 13 (Figures 3f, 4f, 5f, and 6f).

[23] North of 30°N the wind had a more northerly component to the general westerly flow of the southern end of the track. The back trajectories indicated air had passed over Northern China and then along the western side of the Korean peninsula (Figure 7). At 31°N the SO₂ layer with 1 ppbv between 700 and 900 m (Figure 3a) was below the layer of high CO from 1.1 to 2.1 km (Figure 3b). This SO₂ plume was constrained between a weak inversion at 900 m (Figure 3e) and the well mixed layer below 600 m (Figure 3c). At the top of the mixed layer there was a thin cloud layer, which was indicated by the liquid water content
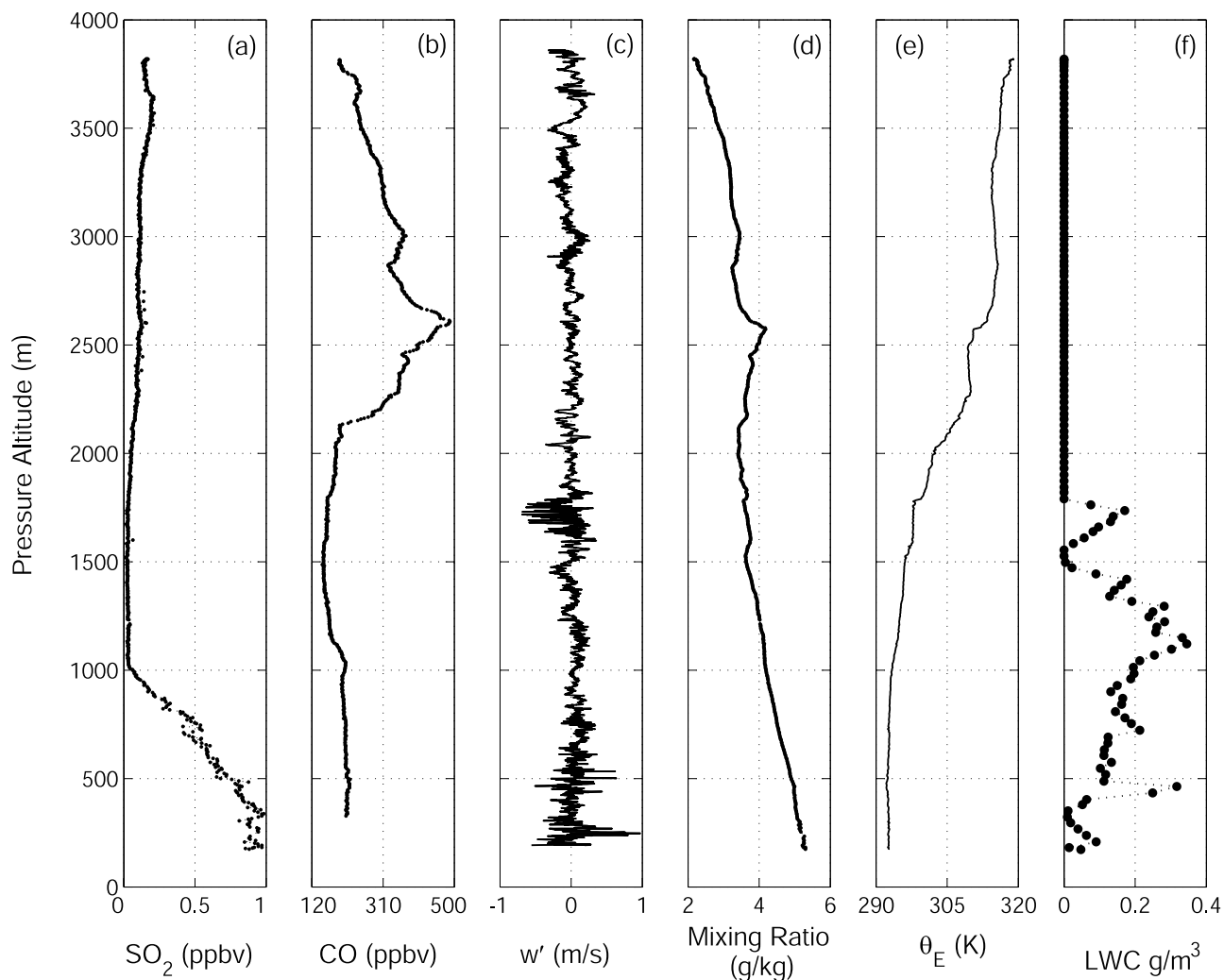
Figure 6. Vertical ascent profiles of (a) SO$_2$, (b) CO, (c) w' (the vertical wind component about the mean vertical wind for the profile shown), (d) water vapor mixing ratio (MR), (e) equivalent potential temperature (θ_e), and (f) liquid water content (LWC) near 124.5°E, 34.8°N for flight 13. Data are 1 Hz except for 10 Hz w' and 0.2 Hz LWC. SO$_2$ appeared to be lost in cloud below 1 km but for 1 to 1.8 km, lower CO compared to above and below indicated an air mass with a different origin (see back trajectory diamonds in Figure 7).

(Figure 3f). The back trajectories near 1 km for this SO$_2$ layer (triangles in Figure 7) descended from above 3 km from the northwest and were over the sea off Shanghai for the day before the flight.

[24] Between 1.2 km and 2 km, where CO exceeded 500 ppbv, the back trajectories descended near the surface over southern China 2–3 days earlier, but the SO$_2$ concentrations of 20–40 pptv were more like those in the mixed layer. With a cloud at 1.8 to 2 km (Figure 3f) and the MR between 1.3 and 2.1 km greater than in the mixed layer, it appeared that there had been rain earlier that reduced the SO$_2$ levels compared to the fresh SO$_2$ plume from Shanghai between 700 and 900 m. Above the cloud SO$_2$ was 60–80 pptv in a region of low turbulence (Figure 3c) and much more stable air (Figure 3e) where CO values were near 200 ppbv. The air above 2 km also had back trajectories to southern China.

[25] The effects of clouds on the SO$_2$ distribution are illustrated by the vertical profiles at 32.7° N, 33.6°N, and

34.8°N (Figures 4a, 5a, and 6a). The wettest cloud encountered on flight 13 was at 32.7°N (Figure 4f). The turbulence data showed that the mixing extended to the cloud top and that the cloud was convective because there were a number of large positive excursions of w' (Figure 4c). The spikes in SO$_2$ in this profile between 400 m and 1 km are positively correlated to the positive excursions of w'. The largest of these updrafts at 1 km corresponded to an SO$_2$ concentration the same as in the lower part of the mixed layer below 400 m. An air parcel with an updraft velocity of 2 m/s would have a transit time of about 5 min from the lower mixed layer at 400 m to 1 km.

[26] At 33.6°N (Figure 5a) a similar situation was encountered where the cloud had nearly dissipated (LWC <0.1 g/m^3, Figure 5f). Below 400 m SO$_2$ is greater than 200 pptv in the mixed layer (Figure 5a), but there were a number of updrafts, which could have produced the structure in the SO$_2$ profile. Above 400 m the turbulence was less intense (Figure 5c), but the structure in the SO$_2$ profile
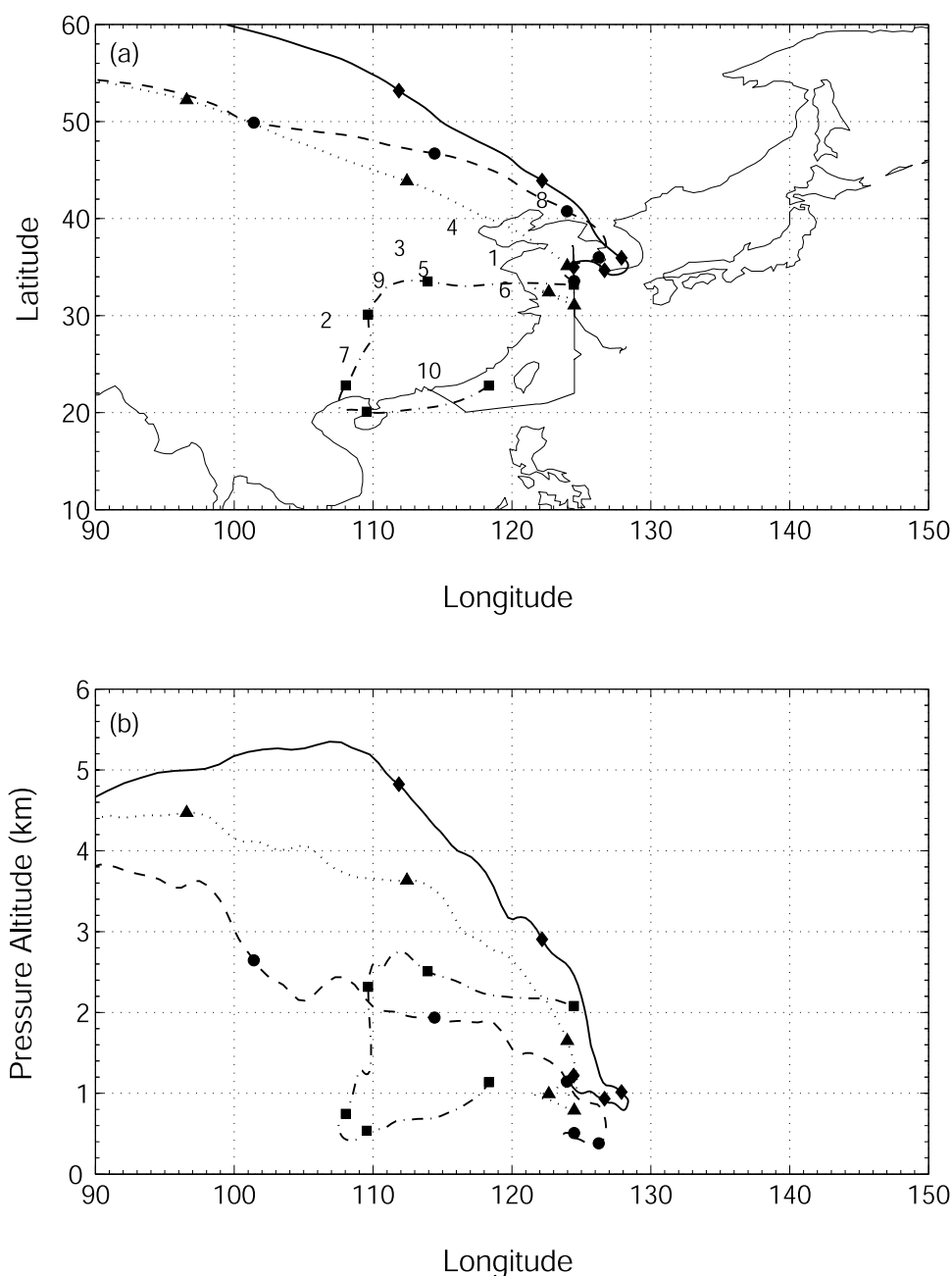
Figure 7. Back trajectories for flight 13 from selected points along the 124.5°E flight relating to the vertical profiles of Figures 3–6: triangles, 31.2°N 800 m; squares, 32.7°N 2 km; circles, 33.6°N 500 m; diamonds, 34.8°N 1.2 km. (a) Horizontal tracks of trajectories with symbols indicating 24-hour periods backward in time from trajectory starting point. Largest regions of SO₂ emissions by rank [*Streets et al.*, 2003]: 1, Shandong; 2, Sichuan; 3, Shanxi; 4, Hebei; 5, Henan; 6, Jiangsu; 7, Guizhou; 8, Liaoning; 9, Shaanxi; 10, Guangdong. (b) Altitude profiles of the back trajectories in Figure 7a with symbols indicating 24-hour periods backward in time from trajectory starting point.

up to 700 m was probably the residual from the convection in the cloud that was dissipating. Drier, less turbulent air with lower CO was above the cloud top at 700 m and appeared to be diluting the moister CO-richer air below causing the cloud to dissipate. At 200 m the SO₂ increased from 200 pptv to 280 pptv, which was what was found on the level leg after the descent. Small jumps in the MR and CO also occurred at 200 m and the concentrations became more uniform below 200 m, which would be

expected in the mixed layer. It appeared that the mixed layer had reestablished at a lower altitude after the cloud began to dissipate.

[27]   At the northern end of the 150 m leg over the Yellow Sea there were clouds extending from 200 m to 1.7 km. Two breaks in the cloud are apparent at 350 m and 1.5 km where the LWC was near zero (Figure 6f). The SO₂ below 400 m varied between 800 to 1000 pptv, and above 400 m SO₂ linearly declined to a minimum of 30 pptv at 1 km. At
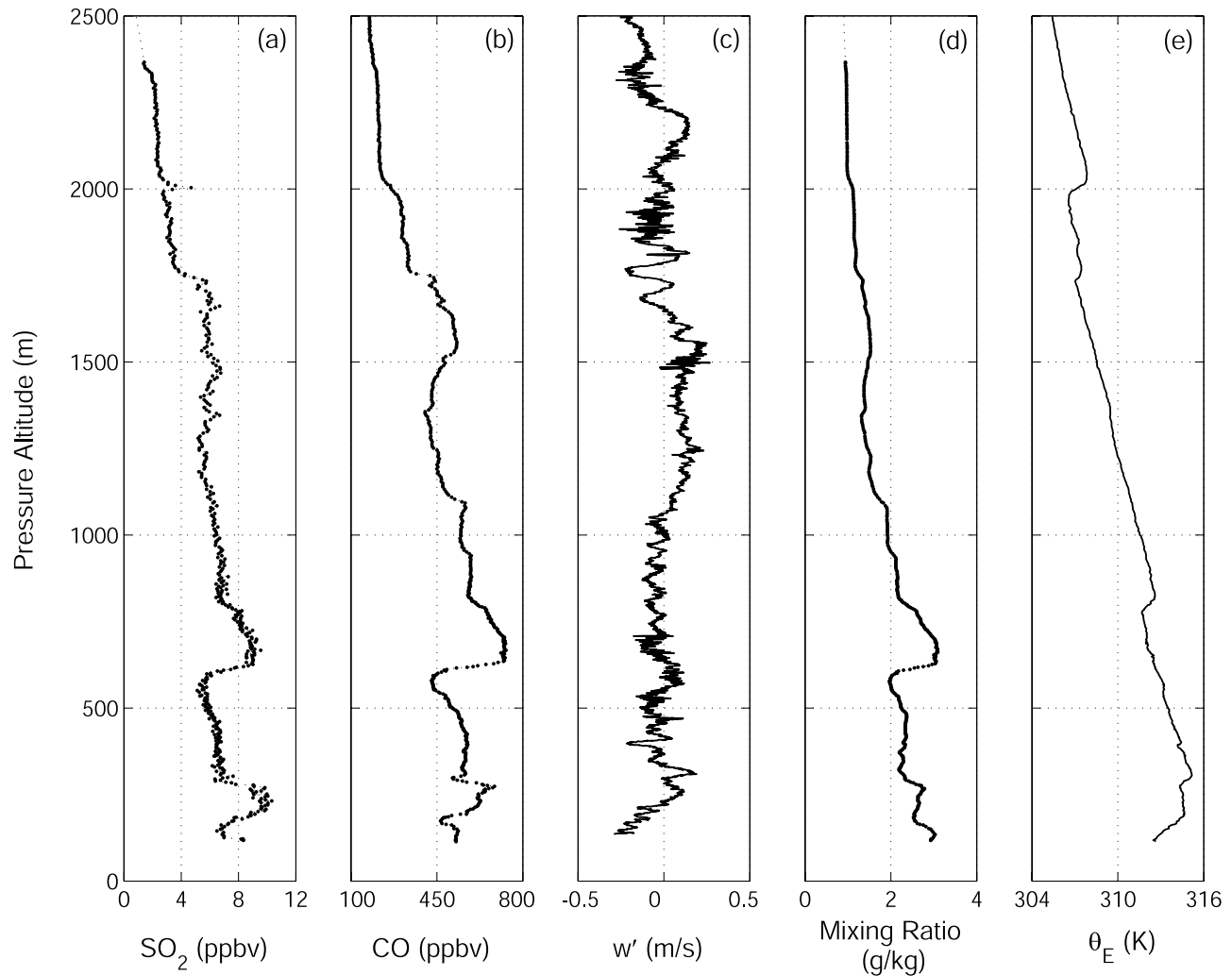
Figure 8. Vertical ascent profiles of (a) SO$_2$, (b) CO, (c) w' (the vertical wind component about the mean vertical wind for the profile shown), (d) water vapor mixing ratio (MR), and (e) equivalent potential temperature (θ_e) near 124.5°E, 35.7°N for flight 14. Data are 1 Hz except for 10 Hz w'. Note that the mixed layer appeared to be below the aircraft at the start of the ascent at 150 m. The air temperature at 150 m was greater than the sea surface temperature.

1.1 km CO also decreased from 210 ppbv to 130 ppbv (Figure 6b) and NO went from >200 pptv to <20 pptv. Although there was a wind shear of 60 degrees from northwest to west at 1.1 km, the air composition appeared more like Northern Hemisphere oceanic air. The back trajectory for 1.3 km indicated that the air had been in the region of the Korean Strait to the east for 2 days (diamond symbol in Figure 7). It is likely that this air mass had been lifted up over the front from the west as part of the warm conveyor belt mechanism [*Jacob et al.*, 2003]. A similar condition had been observed east of Taiwan during PEM West A where the mixed layer was polluted but the air just above was typical of clean marine air from the southeast [*Thornton et al.*, 1996].

3.3. Flight 14

[28] On 18 March 2001 the front had cleared the region of the Yellow Sea and the East China Sea, and there were no clouds along the 124.5°E flight path. The peak SO$_2$ levels were an order of magnitude greater compared to the previous day (Figures 1 and 2). At 36°N, 2–10 ppbv of SO$_2$ was distributed in several layers from near the surface to 2.5 km. A distinct plume of SO$_2$ was observed between 200 m and 300 m from 36°N to 31°N (Figures 8a, 9a, and 10a). A similar plume of CO at those altitudes was observed between 34°N and 36°N (Figures 8b and 9b), which may indicate a common source. At 30°N, SO$_2$ had decreased to <2 ppbv below 600 m (Figure 11a).

[29] The structure of the lower atmosphere for the track along the 124.5°E meridian was very complex. Colder air was descending over 36°N, but at 150 m the air was warmer than the sea surface temperature creating a stratified boundary layer (Figure 8e). Between 35°N and 36°N the aircraft was not completely in the mixed layer at 150 m. At the southern end of the track near 30°N, the sea surface temperature was higher than the air temperature and a well developed mixed layer was established with a depth of 600 m (Figures 11c and 11d) similar to the previous day (Figures 3c and 3d).

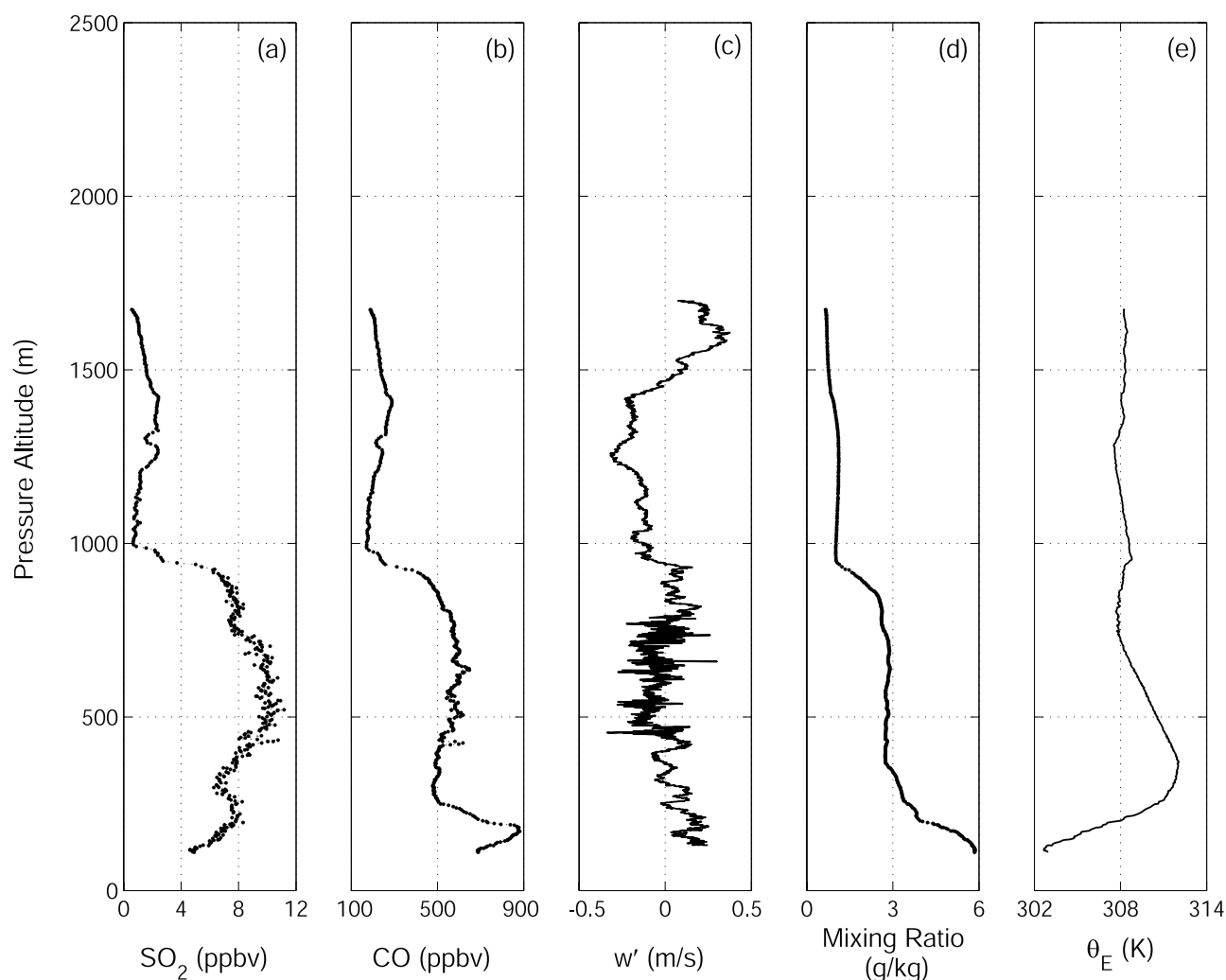[30] The lower troposphere was unstable at 36°N (Figure 8e) with 5 inversions below 2.5 km. Between the

Figure 9. Vertical descent profiles of (a) SO$_2$, (b) CO, (c) w' (the vertical wind component about the mean vertical wind for the profile shown), (d) water vapor mixing ratio (MR), and (e) equivalent potential temperature (θ_e) near 124.5°E, 34.2°N for flight 14. Data are 1 Hz except for 10 Hz w'. On the basis of the MR and θ_e the mixed layer top was very near 150 m, but the variance in w' does not indicate much mixing.

inversions at 0.8 and 1.7 km SO$_2$ was a nearly constant at 6 ppbv (Figure 8a). This layer appeared to be constrained between the inversions at 800 m and 1.7 km and the profiles of CO (Figures 8b), water vapor (Figure 8e), and ozone also had abrupt changes at these two altitudes. The slow meandering of w' in this layer was more characteristic of the free troposphere than the boundary layer.

[31] The distinct plume of SO$_2$ and CO between 600 and 800 m (Figures 8a and 8b) also contained NO > 200 pptv, indicating a fresh pollution plume. This air was also nearly 50% moister than the air above or below (Figure 8d). The plume appeared to be trapped between the inversion at 800 m and a shear layer near 600 m, which is reflected in w' (Figure 8c). These northern SO$_2$ plumes at 36°N all had back trajectories to the Hebei region in one day (Figure 12, inverted triangles and right pointing triangles).

[32] From 31°N to 36°N a well-defined SO$_2$ layer existed between 200 and 300 m (Figures 8a, 9a, and 10a). This plume was below the inversions that were near 400 m at 31°N and 300 m at 35.7°N (Figures 8e, 9e, and 10e).

Between 34°N and 35.7°N the fight path did not descend low enough to remain in the mixed layer. It is clear from the turbulence (Figures 9c and 8c) and θ_e (Figures 9e and 8e) that the flight path was still above the mixed layer at 150 m. The sea surface temperature had decreased 2 K between 31°N and 36°N while the air temperature remained nearly the same. North of 35°N the air temperature was greater than the sea surface temperature. With the warmer air above the colder sea this part of the boundary layer became stable, particularly between 34°N and 36°N, where the turbulence below 400 m (Figures 8c and 9c) is more like the free troposphere than a well mixed boundary layer. On the basis of the turbulence data (Figures 8c and 9c) and the MR data (Figures 8d and 9d), it appeared that the aircraft did not descend low enough to be completely in the mixed layer at 150 m between 35°N and 36°N. The high variability observed for SO$_2$ on the level leg at 150 m at 35.4°N (Figure 2d) was probably caused by the aircraft path going in and out of the mixed layer and the plume above the mixed layer top.
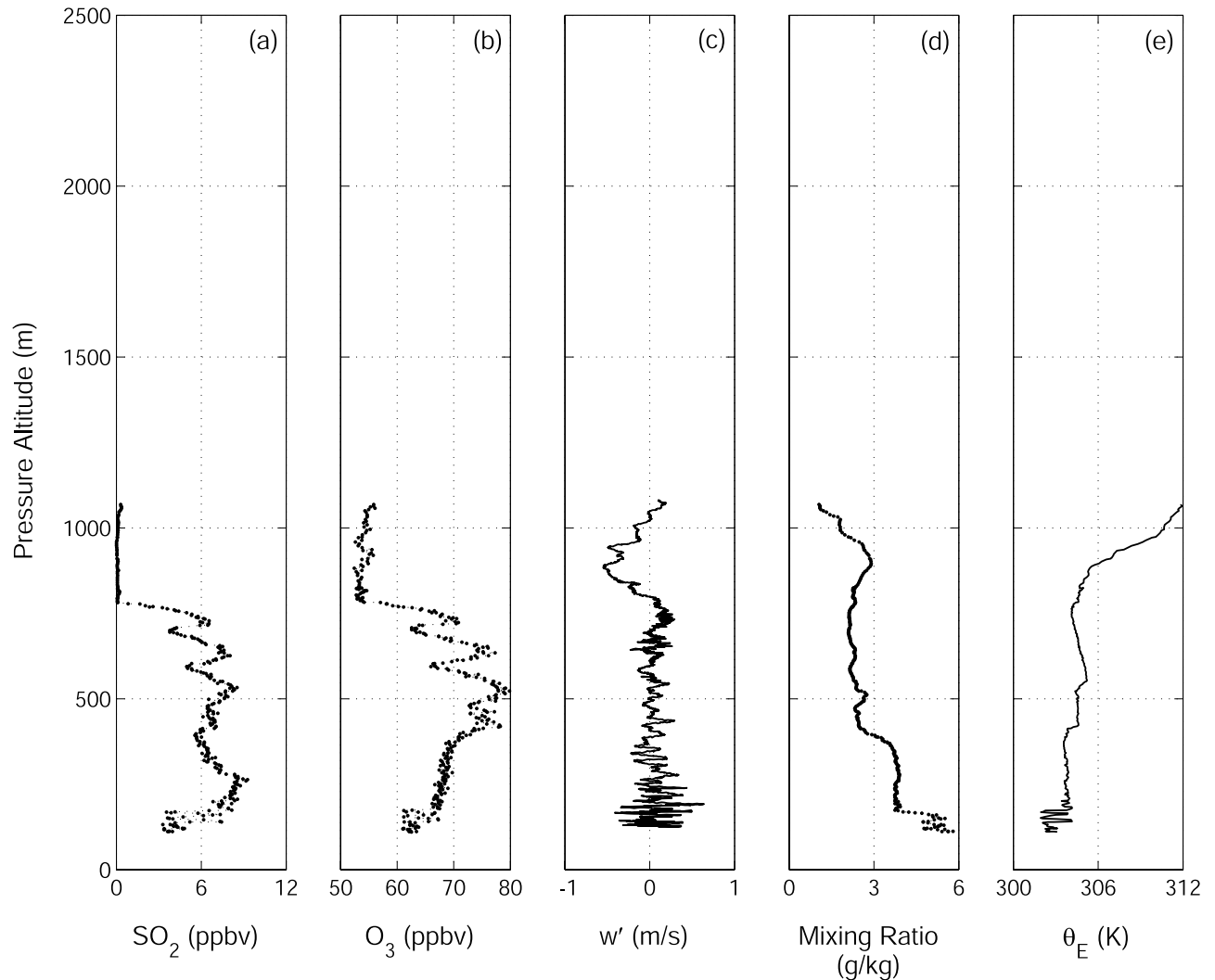
Figure 10. Vertical descent profiles of (a) SO₂, (b) O₃, (c) w' (the vertical wind component about the mean vertical wind for the profile shown), (d) water vapor mixing ratio (MR), and (e) equivalent potential temperature (θ_e), near 124.5°E, 31.1°N for flight 14. Data are 1 Hz except for 10 Hz w'. The variances for w', θ_e, and MR indicate that the mixed layer was near 170 m. Note the sharp decreases in SO₂ and CO at 800 m where the turbulence becomes small.

[33] At 34.2°N, θ_e indicated an air mass above 1 km with neutral stability (Figure 9e). Both SO₂ and CO between 1 and 1.7 km at 34.2°N (Figures 9a and 9b) were half their concentrations at 36°N. The back trajectories for the SO₂ between 1 and 2 km all passed north of the Shandong peninsula (37°N), but the air parcels descended from above 3 km to the aircraft position. The air parcels below 1 km on the aircraft track had come from the region of 115°E, 35°N within 1.5 days and remained below 1.5 km (Figure 12, squares). That region contains three major point sources in southern Shandong and northwestern Jiangsu [Streets et al., 2003].

[34] At 31.1°N the turbulent mixing was stronger below 400 m, but in this area the flight path appeared to be crossing through a sloped mixed layer top that was uneven. On the basis of the rapid oscillations in SO₂, w', θ_e (Figure 10 below 200 m) and the Lyman α fast water vapor sensor, the flight path was probably in and out of the top of the mixed layer. There was a sharp drop in SO₂

from 8 ppbv above 200 m to about 4 ppbv below 200 m (Figure 10a). It appeared that SO₂ from the plume between 200 and 400 m was isolated from the mixed layer.

[35] Between 31.1°N and 30.2°N, SO₂ at 150 m steadily decreased from 3 to 1.5 ppbv (Figure 2d). At the southern end of the flight track at 30°N the mixed layer was 600 m deep (Figures 11b, 11d, and 11e) compared to about 200 m at 31°N. The decrease in SO₂ from 31°N to 30°N at 150 m was related in part to the increase in the mixed layer depth (Figures 10b and 11b). The sea surface temperature had increased by 2 K from the north to the south, which would have increased the heating of the mixed layer.

[36] The vertical profile at 30°N was to the east of the 124.5°E meridian at the end of the flight pattern in this region. There was a well defined top to the mixed layer (Figures 11c and 11d) where there was a sharp decrease in SO₂ (Figure 11a) and the very stable air mass above 600 m (Figure 11e) where SO₂ decreased to 40 pptv. The SO₂ plume between 1.4 km and 1.6 km at 30°N (Figure 11a) was
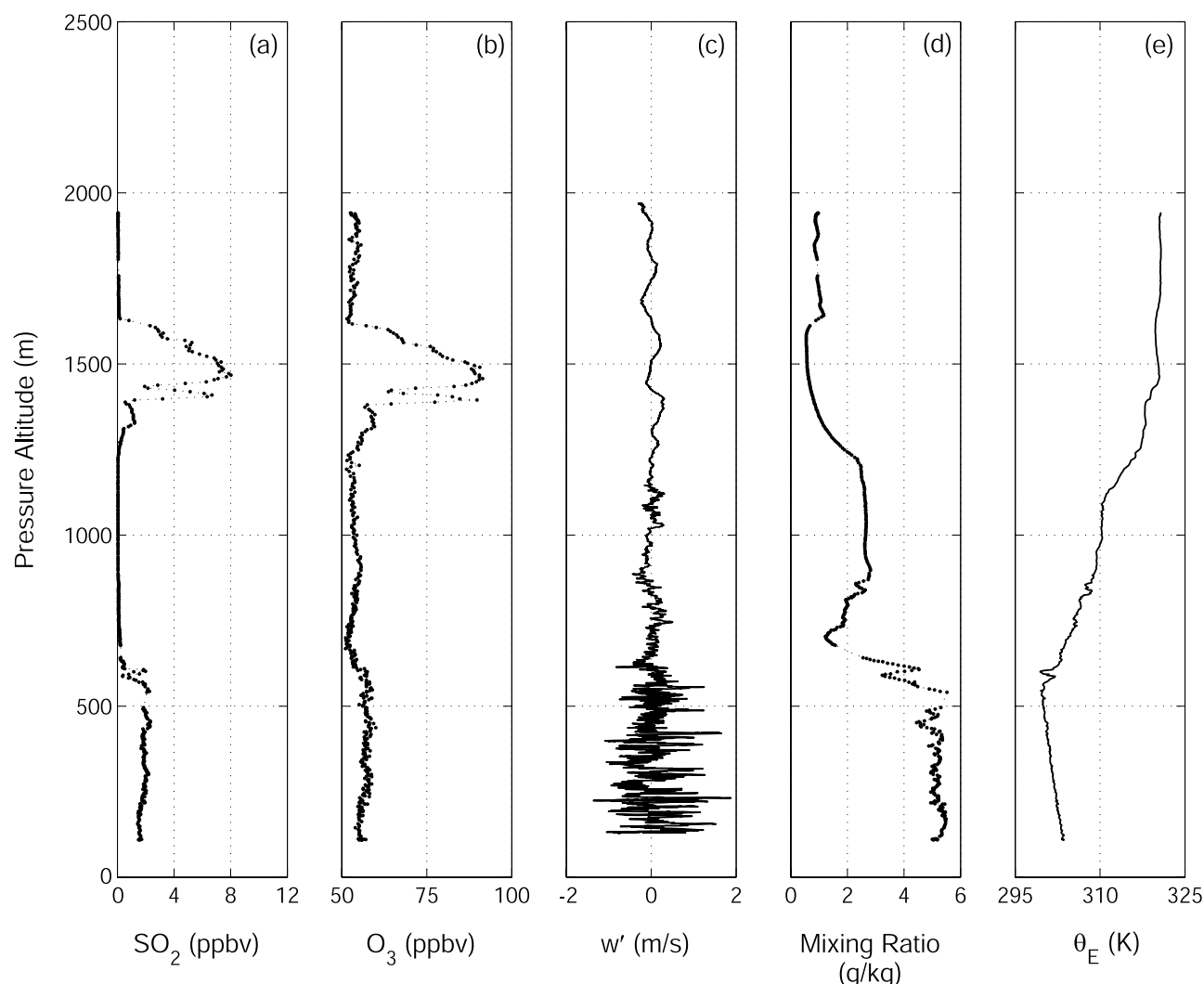
Figure 11. Vertical ascent profiles of (a) SO_2, (b) O_3, (c) w' (the vertical wind component about the mean vertical wind for the profile shown), (d) water vapor mixing ratio (MR), and (e) equivalent potential temperature (θ_e), near 124.5°E, 30.2°N for flight 14. Data are 1 Hz except for 10 Hz w'. At this southern end of the flight track a well-developed mixed layer of 600 m has evolved. The SO_2 and O_3 plume around 1.5 km is in a relatively dry, nonturbulent air parcel that had recently descended from 4 km (see trajectory with circles in Figure 12).

in an air mass of neutral stability (Figure 11e) with very low turbulence (Figure 11c). The structural features of this SO_2 profile were also present for O_3 (Figure 11b) and NO, and water vapor had decreased to <0.6 g/kg compared to >1 g/kg above 1.6 km and >2.5 g/kg below 1.3 km. On the basis of the back trajectories, the SO_2 plume at 30°N came from the southern side of the Shandong peninsula (Figure 12, circles). The back trajectories indicated air parcels that rapidly descended from above 3 km, which is consistent with θ_e >320 K above 1.5 km at 30°N (Figure 11e). This descending air mass appeared to have trapped and constrained the SO_2 pollution plume.

4. Discussion

[37] The transport of SO_2 for these two flights over the East China Sea-Yellow Sea region was very varied within the boundary layer as well as above it. Transport occurring above the boundary layer is not surprising given the convective activity of early spring over the East Asia basin and the generally westerly winds [*Fuelberg at al.*, 2003]. However, the transport was often in well defined layers that were constrained by the lack of vertical mixing and by the thermodynamic structure. These plumes appeared to maintain their structure well away from the coast of Asia under conditions described by *Cho et al.* [2003] and *Thornton et al.* [2002b].

[38] The most unusual part of the SO_2 plume structure was just above the mixed layer top and in the mixed layer. For these two flights with greatly different SO_2 concentrations, the structure of boundary layer was also different. There was a well mixed layer close to the sea surface for both flights but the depth was much less for flight 14 except at 30°N. The greater depth (600–1000 m) for flight 13 was related to the clouds of varying heights. Above the well mixed layer there was a less well mixed layer but still below
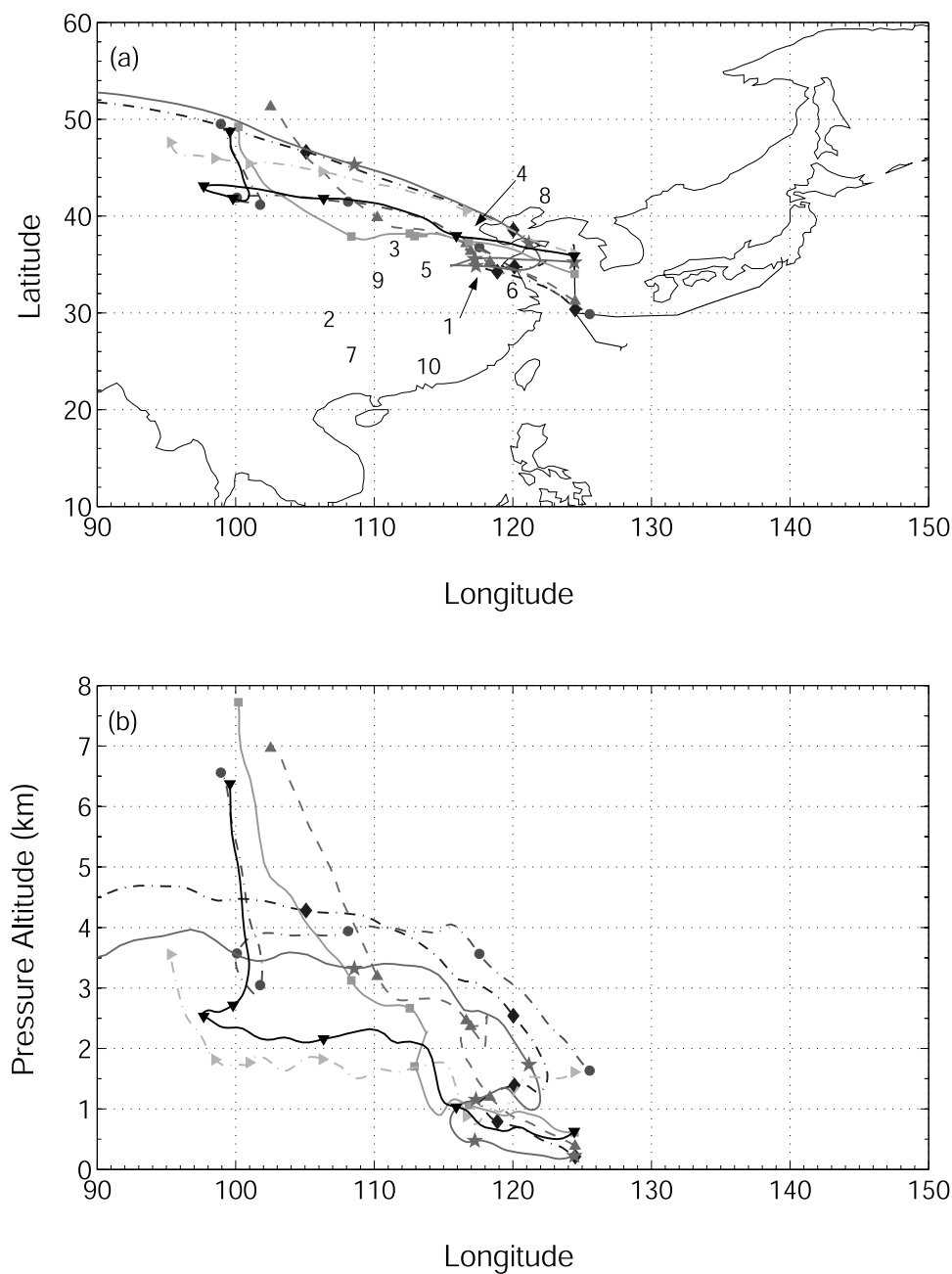
Figure 12. Back trajectories for flight 14 from selected points along the 124.5°E flight relating to the vertical profiles of Figures 8–11: inverted triangles, 35.7°N 650 m; right pointing triangles, 35.7°N 1.6 km; star, 34–36°N 150 m; squares, 34.2°N 600 m; triangles, 31.1°N 400 m; diamonds, 30–31°N 150 m; circles, 30.2°N 1.6 km. (a) Horizontal tracks of trajectories with symbols indicating 24-hour periods backward in time from trajectory starting point. Largest regions of SO$_2$ emissions by rank [*Streets et al.*, 2003]: 1, Shandong; 2, Sichuan; 3, Shanxi; 4, Hebei; 5, Henan; 6, Jiangsu; 7, Guizhou; 8, Liaoning; 9, Shaanxi; 10, Guangdong. (b) Altitude profiles of the back trajectories in Figure 12a with symbols indicating 24-hour periods backward in time from trajectory starting point.

a temperature inversion or a major decrease in water vapor that usually marks transition to the free troposphere.

[39] During flight 13 the SO$_2$ was found to be transported from the continent in the well mixed layer as well as in cloud but in decreasing amounts from the Yellow Sea in the north to the East China Sea in the south. The SO$_2$ observed in clouds was mixed by convection into the cloud from the SO$_2$ rich air below. One of the limits to SO$_2$ uptake in cloud is the availability of hydrogen peroxide (H$_2$O$_2$). With ppbv levels of SO$_2$ at the northern end, heterogeneous loss of SO$_2$ to cloud droplets may have been limited by the depletion of H$_2$O$_2$ by the SO$_2$. The remaining primary loss process is by O$_3$, which has limited solubility in water and a much lower rate of reaction. It is difficult to assess the cloud

loss rate of SO$_2$ because this experiment was not designed to study clouds so that the effects of dilution could not be ascertained.

[40] The SO$_2$ plumes in the lower free troposphere of flight 13 were like the plumes above the well mixed layer for flight 14. In both cases the plumes were in air masses with lower turbulence and with high to neutral stability. The SO$_2$ plumes at 31°N and 32.7°N (Figures 3a and 4a) may have been the leading edge of the air mass filling in behind the front that cleared the region late in the day. This air mass movement was above the stratus cloud decks although it may have been affected by precipitation on the previous day.

[41] During flight 14 over the Yellow Sea it appeared that the transport from surface sources near the coast occurred when the continental air moved offshore over the marine boundary layer. The marine mixed layer depth (<150 m) was constrained by the cold surface temperature and the warmer air above (Figures 8e and 9e). Even though it was early spring, the continental boundary layer was deeper than the marine boundary layer because the highly populated landmass contributed to the diabatic heating over land. The structure of the plumes north of 31°N was related to the turbulence structure between 200 m and 1000 m (Figures 8c, 9c, and 10c). The apparent oscillations in the SO$_2$ (Figures 8a, 9a, and 10a) were also seen for O$_3$ and NO. These oscillations corresponded to the meanders of the vertical velocity (Figures 8c, 9c, and 10c). The other extreme in turbulence is seen in the region between 450 and 750 m (Figure 9c) where the turbulence mixed the chemical species to nearly uniform concentrations in this layer (Figures 9a and 9b).

[42] The observation that transport between the mixed layer and the layer above can be dynamically limited introduces a possible scenario of why SO$_2$ can persist in low level plumes over the ocean [*Thornton et al.*, 2002b]. When the vertical transport is controlled by entrainment processes, then mixing occurs on much slower timescales than when mixing is determined by convection. When entrainment is controlling the transport of SO$_2$ to the sea surface, the loss of SO$_2$ to sea salt aerosol near the surface and to the surface itself becomes limited. If this dynamic control is not included in transport models, an overestimation of SO$_2$ heterogeneous loss to the sea or aerosol would be likely. The same would be true when the SO$_2$ plumes are just above the boundary layer top where the mixing processes appeared to be limited by the colder air masses descending over the marine boundary layer. Investigation of these possibilities for contributing to long range transport over the Pacific will be presented separately.

[43] By looking at the ethyne (C$_2$H$_2$) (D. R. Blake, TRACE-P data archive) to CO ratio we can get an estimate of the age of the air relative to its photochemical decay and dilution by mixing [*McKeen and Liu*, 1993; *McKeen et al.*, 1996; *Sandholm et al.*, 1992, 1994; *Smyth et al.*, 1996]. Above 2.5 km the relationship of SO$_2$ to the C$_2$H$_2$/CO was similar for both flights. For the most recent encounters of the pollution plumes (C$_2$H$_2$/CO > 3), SO$_2$ was increasing with increasing C$_2$H$_2$/CO (Figures 13a and 13c). These SO$_2$ samples were all from the region north of 33°N. When C$_2$H$_2$/CO was <3 above 2.5 km, SO$_2$ was generally <50 pptv. For flight 13 the low SO$_2$ concentrations with

C$_2$H$_2$/CO > 3 were consistent with SO$_2$ being significantly reduced by heterogeneous processing by precipitation and clouds on the day prior to the encounter with the aircraft. The low SO$_2$ values for flight 14 with C$_2$H$_2$/CO < 3 were all from the region south of 32°N. While the lower values of C$_2$H$_2$/CO indicate longer time for processing, the low SO$_2$ concentrations may have been reduced by the cloud and heterogeneous processing during the periods of precipitation between 27°N and 32°N over the sea on 15 March 2001, two days before the encounter with the aircraft.

[44] Below 2.5 km heterogeneous processing of SO$_2$ by clouds, precipitation, and sea salt aerosol, and the sea surface would be more likely. This is clearly seen for flight 13 at all values of C$_2$H$_2$/CO when SO$_2$ was <100 pptv (Figure 13b). For the northern end of the flight track in the Yellow Sea, the SO$_2$ concentrations >200 pptv were in the plume moving from north to south (Figure 2b) with C$_2$H$_2$/CO between 3.5 and 4, which would have been within one day of transport from the source to the encounter with the aircraft. A similar relationship of SO$_2$ with C$_2$H$_2$/CO was seen for flight 14 when all of the plumes below 2.5 km described above were within 1.5 days transport from the source (Figure 12). Here the range of SO$_2$ concentrations more likely represents the source variations.

5. Model Comparison

[45] The CFORS/STEM-2K1 modeling system as used in the TRACE-P and Ace-Asia experiments was built within the RAMS mesoscale meteorological model [*Pielke et al.*, 1992]. The CFORS component contained multiple tracers run online in RAMS, so that all the online meteorological information such as three-dimensional (3-D) winds, boundary layer turbulence, surface fluxes and precipitation amount are directly used by the tracer model at every time step. As a result, CFORS produces with high time resolution 3-D fields of tracer distributions and major meteorological parameters. For the analysis of reactive species, a chemical transport model (CTM) is used. In this paper we discuss results using the STEM model. The STEM version used is referred to as the 2K1 (2001) version (thus STEM-2K1). CFORS provides the meteorological fields used by STEM, and then STEM calculates the transport, chemistry, removal, and photolysis processes. The important new features in STEM-2K1 include (1) the use of the SAPRC99 chemical mechanism [*Carter*, 2000], which consists of 93 species and 225 reactions; (2) the integration of the chemical mechanism using the implicit second-order Rosenbrock method [*Sandu et al.*, 1997]; (3) the calculation of photolysis rates online, considering the influences of cloud, aerosol and gas-phase absorptions due to O$_3$, SO$_2$ and NO$_2$, using the NCAR Tropospheric Ultraviolet-Visible (TUV) radiation model [*Madronich and Flocke*, 1999]; and (4) the extension of the aerosol calculations to include optical information (e.g., extinction) in addition to mass, size and composition. Complete details regarding this model are available from *Carmichael et al.* [2003], and *Uno et al.* [2003]. Boundary conditions were selected based on observational data, and they were set to the lowest 5% at each altitude of the values observed during the TRACE-P operations in the western Pacific. The numerical model domain for the analysis (both CFORS and STEM) was centered at
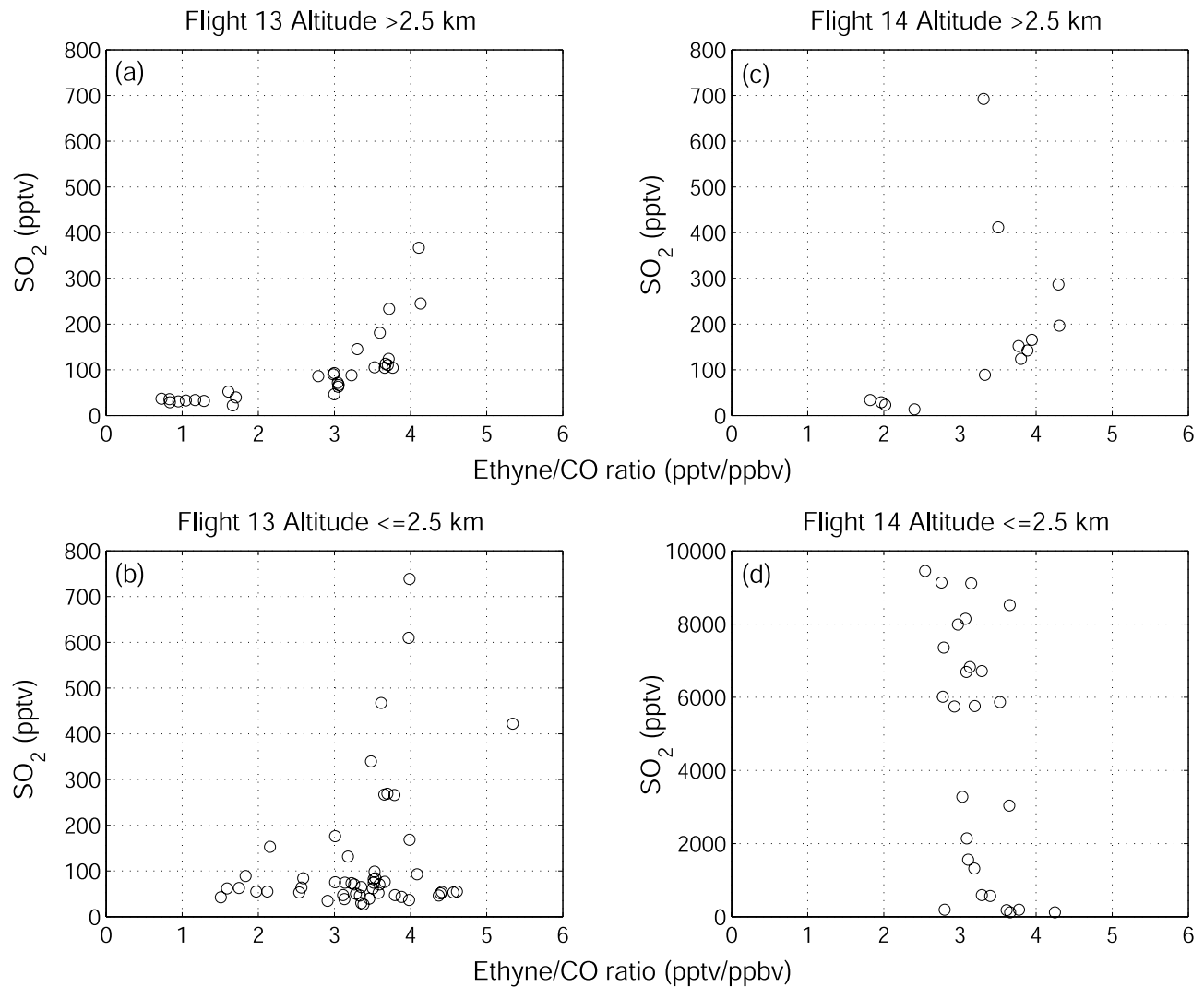
Figure 13. SO₂ as a function of the ethyne to CO ratio (a) and (c) above and (b) and (d) below 2.5 km pressure altitude for flights 13 (Figures 13a and 13b) and 14 (Figures 13c and 13d) along the 124.5°E flight path. The 1 Hz data for SO₂ and CO were integrated over the time period of the ethyne samples.

25°N, 115°E with a horizontal grid of 100 by 90 grid points and a resolution of 80 km. In the vertical, the domain was divided into 23 layers (nonuniformly spaced layers ranging in depth from 150 to 1800 m), with the top level at 23 km. All calculations were performed on Linux clusters.

[46] The SO₂ observations and the results of the CFORS/STEM-2K1 model [*Carmichael et al.*, 2003] along the path for the entire P-3B flight 13 are shown in Figure 14. The time period when the flight track was along 124.5°E is 0315 to 0805 UTC. The model closely followed the SO₂ data at all altitudes before 0400 UTC, which was mostly in the area between Hong Kong and Taiwan. That region had not received any precipitation for at least 4 days prior to the flight (Global Precipitation Climatology Project, Laboratory for Atmospheres, NASA Goddard Space Flight Center, http://precip.gsfc.nasa.gov/rain_pages/daily_choice.html).

[47] After 0400 UTC, the model results exceeded the SO₂ observations at all altitudes by factors of 2 to 20. The vertical distribution of the model had SO₂ > 0.5 ppbv at all altitudes above 0.5 km between 0430 and 0530 UTC which

were not observed. Between 0600 and 0730 UTC the model trend was the same as the observations, but the model results were higher by an order of magnitude compared to the observations. As described above, the observations indicate that a large fraction of SO₂ had likely been removed by heterogeneous processing prior to flight 13, particularly below 2 km.

[48] Near the end of flight 13, away from the flight track in the Yellow Sea, the model had SO₂ concentrations near 1 ppbv at 3.1 km while the observations were that the SO₂ was 0.1 ppbv. Above 3 km the model results were <100 pptv, but the observations showed a 500 pptv layer about 4.4 km with concentrations above and below of >200 pptv. The model accurately predicted the 250 ppbv CO for the 3 km leg, but it under predicted the 100 ppbv CO and the 55 ppbv ozone at 5.5 km. The SO₂ concentrations of 200 pptv at 5.5 km were much higher than expected based on the C₂H₂/CO ratio of 1.3 for other data along 124.5°E (Figure 2a). Most of the back trajectories at 5.5 km passed over northern India above 5 km 2 days earlier and
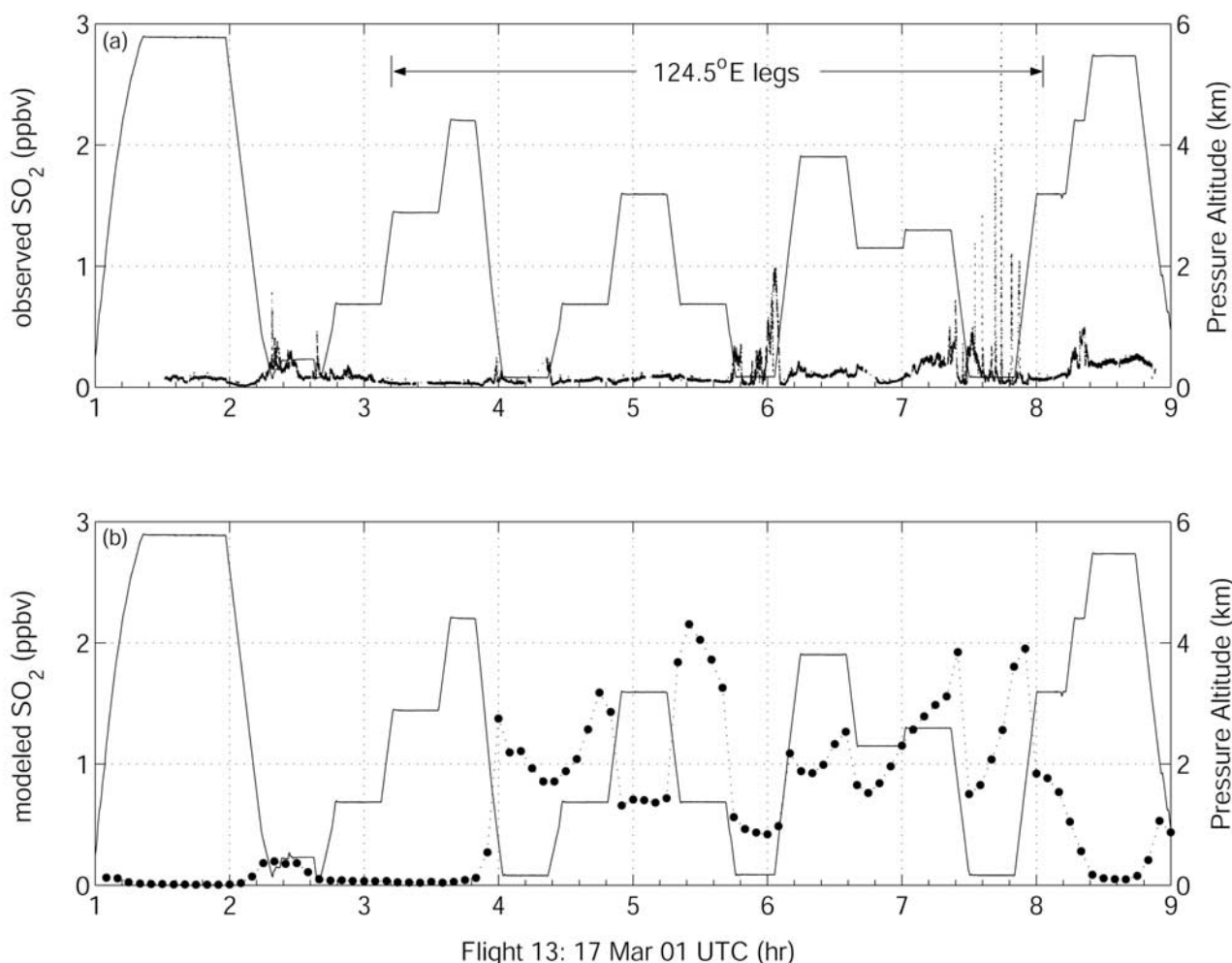
Figure 14. Time series for (a) the SO₂ observations and (b) the CFOR/STEM-2K1 chemical transport model for flight 13. The solid line is the aircraft flight path. Flight track was along 124.5°E from 0315 to 0805 UTC. Spikes in observed SO₂ at 150 m between 0730 and 0750 UTC were from fresh ship plumes.

descended to 2–4 km over central and southern Sudan 5 days earlier. The only likely significant SO₂ source would be oil refineries in central Sudan and in the oilfields of southern Sudan. This would be consistent with the C₂H₂/CO ratio and the 0.5% sulfur content of the oil [http://www.eia. doe.gov/emeu/cabs/sudan.html]. In this case the source was out of the model domain for this field study.

[49] The model gave better agreement with the SO₂ observations on flight 14, particularly on the flight legs below 1 km. The model significantly overestimated the SO₂ for the 1.5 to 2.5 km levels. One low level feature the model missed was the decrease in SO₂ as the flight path turned east from 124.5°E toward Japan (about 0600 UTC in Figure 15). The model similarly overestimates SO₂ on a 150 m leg off the coast of Japan at 0800 UTC, although the model accurately predicted the 240 ppbv of CO.

[50] If precipitation was the primary cause of the model overestimating the SO₂ for flight 13, the model should have done better on flight 14 for those altitudes between 1.5 and 2.5 km. We believe that the dynamics (described above) resulted in this deviation. At the northern end of the Yellow Sea flight path (0330–0400 UTC), the model exceeded the SO₂ observations by a factor of 3–4 (Figure 15). Near 2 km

on either side of the southern 150 m leg (0500–0530 UTC and 0615–0645 UTC) the model overestimated the observed SO₂ by a factor of 7–10. It appears that the model did not capture the dynamics properly and expanded to higher altitude the plumes that lay below 2 km. At the northern end the profile showed unstable regions capped by inversions with enhanced turbulence just below 2 km (Figure 8c). At the southern end the atmosphere had neutral stability but there was virtually no turbulence. With no turbulence it would be less likely that the 200 m thick SO₂ plume at 1.5 km (Figure 11a) would be diffused [Cho et al., 2003]. Here the scale of the SO₂ feature was too small for the model resolution.

[51] The reasons for the poorer performance of the model under cloudy conditions remain an open question. However, from detailed analysis of model performance related to photochemical processes, including the calculation of photolysis rates and a number of the species active within the photochemical oxidant cycle (e.g., OH, HCHO, PAN, O₃), this problem does not appear to be associated with deficiencies in the gas phase mechanism. It is possible that there are some issues related to cloud chemistry, however, the fine-scale turbulence structure that was observed was not ade-
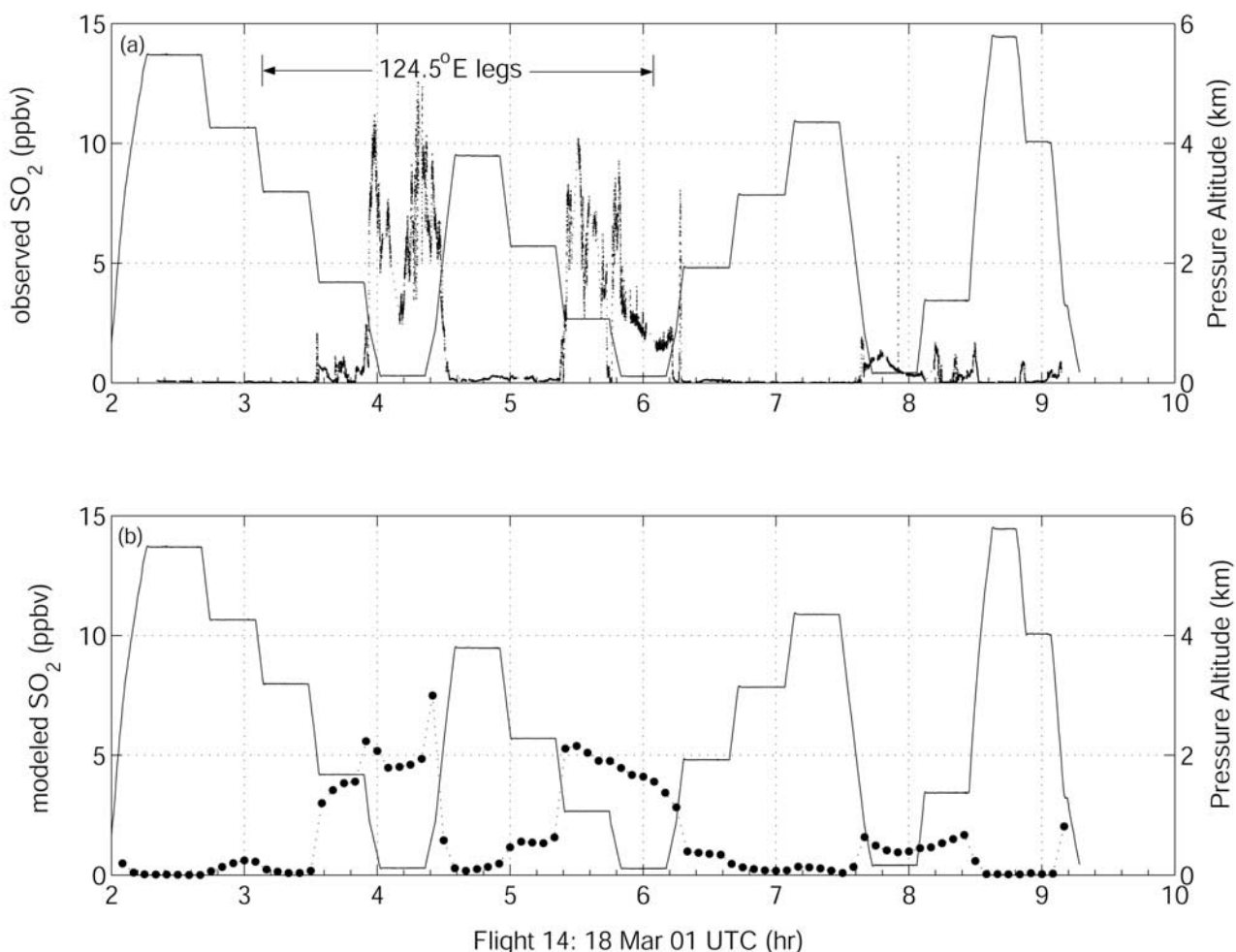
Figure 15. Time series for (a) the SO₂ observations and (b) the CFOR/STEM-2K1 chemical transport model for flight 14. The solid line is the aircraft flight path. Flight track was along 124.5°E from 0307 to 0605 UTC.

quately resolved in our present modeling analysis. A more detailed treatment of the dynamics in the continental/marine transition region, and finer vertical resolution in the CFORS meteorological analysis, are required to more accurately capture this behavior. This line of study is now underway.

6. Conclusion

[52] During the P-3B flights over the Yellow Sea much of the transport and distribution of SO₂ can be understood in the context of the dynamics and thermodynamics of the atmosphere. As might be expected, the meteorological complexity is high during the transition from winter to early spring near the coast of the East Asian continent because of the differences in temperature between land and sea and frequent frontal passage. It was clear that precipitation near the coast had a major effect on decreasing SO₂ transported to the Pacific Ocean at low altitudes. However, in the air masses following frontal passage, significant amounts of SO₂ were transported between 0.5 and 2 km.

[53] In the subsiding air behind the front, high concentrations of SO₂ were transported significant distances above the marine mixed layer. The SO₂ transport occurred in layers

defined by low turbulent mixing that were often constrained by temperature inversions. In several cases discussed here, SO₂ layers were immediately above the marine mixed layer. In the absence of convective mixing, the relatively slow process of entrainment limited the transport of SO₂ into the marine mixed layer and, consequently, to heterogeneous loss to the sea surface and sea salt aerosols. Further investigation of the TRACE-P data is underway to evaluate the role of the atmospheric dynamics in the long range transport of Asian SO₂ across the North Pacific.

[54] When the CFORS/STEM-2K1 regional-scale chemical transport model is compared to observations over a two day period that represented the extremes of the spring transport, it was clear that the poor agreement was related to the treatment of the dynamics on the SO₂ distributions. Some features were on scales that were not within the resolution of the model. The major deviations of the model from the observations were in the mixed layer on the day of the frontal passage and in the 1.5 to 2.5 km range for both wet and dry conditions.

References

Bandy, A. R., D. C. Thornton, and A. R. Driedger III, Airborne measurements of sulfur dioxide, dimethyl sulfide, carbon disulfide, and carbonyl sulfide by isotope dilution gas chromatography/mass spectrometry, *J. Geophys. Res.*, *98*(D12), 23,423–23,433, 1993.

Carmichael, G. R., et al., The MICS-Asia study: Model intercomparison of long-range transport and sulfur deposition in East Asia, *Atmos Environ*, *36*(2), 175–199, 2002.

Carmichael, G. R., et al., Regional-scale chemical transport modeling in support of intensive field experiments: Overview and analysis of the TRACE-P observations, *J. Geophys. Res.*, *108*(D21), 8823, doi:10.1029/2002JD003117, in press, 2003.

Carter, W., Documentation of the SAPRC-99 chemical mechanism for voc reactivity assessment, Final report to California Air Resources Board contract no. 92–329, Univ. of Calif., Riverside, 8 May 2000.

Chin, M., D. L. Savoie, B. J. Huebert, A. R. Bandy, D. C. Thornton, T. S. Bates, P. K. Quinn, E. S. Saltzman, and W. J. DeBruyn, Atmospheric sulfur cycle simulated in the global model GOCART: Comparison with field observations and regional budgets, *J. Geophys. Res. Atmos.*, *105*(D20), 24,689–24,712, 2000.

Cho, J., R. E. Newell, B. E. Anderson, J. D. Barrick, and K. L. Thornhill, Characterizations of tropospheric turbulence and stability layers from aircraft observations, *J. Geophys. Res.*, *108*(D20), 8784, doi:10.1029/2002JD002820, in press, 2003.

Fuelberg, H. E., R. O. Loring Jr., M. V. Watson, M. C. Sinha, K. E. Pickering, A. M. Thompson, G. W. Sachse, D. R. Blake, and M. R. Schoeberl, TRACE A trajectory intercomparison: 2. Isentropic and kinematic methods, *J. Geophys. Res.*, *101*(D19), 23,927–23,939, 1996.

Fuelberg, H. E., C. M. Kiley, J. R. Hannan, D. J. Westberg, M. A. Avery, and R. E. Newell, Meteorological conditions and transport pathways during the transport and chemical evolution over the Pacific (TRACE-P) experiment, *J. Geophys. Res.*, *108*(D20), 8782, doi:10.1029/2002JD003092, in press, 2003.

Hoell, J. M., D. D. Davis, S. C. Liu, R. Newell, M. Shipham, H. Akimoto, R. J. McNeal, R. J. Bendura, and J. W. Drewry, Pacific exploratory mission-west A (PEM-West A): September–October 1991, *J. Geophys. Res.*, *101*(D1), 1641–1653, 1996.

Hoell, J. M., D. D. Davis, S. C. Liu, R. E. Newell, H. Akimoto, R. J. McNeal, and R. J. Bendura, The Pacific Exploratory Mission-West phase B: February–March, 994, *J. Geophys. Res.*, *102*(D23), 28,223–28,239, 1997.

Jacob, D. J., J. Crawford, M. M. Kleb, V. S. Connors, R. J. Bendura, J. L. Raper, G. W. Sachse, J. Gille, L. Emmons, and J. C. Heald, Transport and chemical evolution over the Pacific (TRACE-P) mission: Design, execution, and first results, *J. Geophys. Res.*, *108*(D20), 8781, doi:10.1029/2002JD003276, in press, 2003.

Kim, B.-G., J.-S. Han, and S.-U. Park, Transport of SO$_2$ and aerosol over the Yellow Sea, *Atmos. Environ.*, *35*, 727–737, 2001.

Madronich, S., and S. Flocke, The role of solar radiation in atmospheric chemistry, in *Handbook of Environmental Chemistry*, edited by P. Boule, pp. 1–26, Springer-Verlag, New York, 1999.

McKeen, S. A., and S. C. Liu, Hydrocarbon ratios and photochemical history of air masses, *Geophys. Res. Lett.*, *20*, 2363–2366, 1993.

McKeen, S. A., S. C. Liu, E.-Y. Hsie, X. Lin, J. D. Bradshaw, S. Smyth, G. L. Gregory, and D. R. Blake, Hydrocarbon ratios during PEM-West A: A model perspective, *J. Geophys. Res.*, *101*, 2087–2109, 1996.

Pielke, R. A., et al., A comprehensive meteorological modeling system-RAMS, *Meteorol. Atmos. Phys.*, *49*, 69–91, 1992.

Russell, L. M., D. H. Lenschow, K. K. Laursen, B. Krummel, S. T. Siems, A. R. Bandy, D. C. Thornton, and T. S. Bates, Bidirectional mixing in an ACE 1 marine boundary layer overlain by a second turbulent layer, *J. Geophys. Res.*, *103*, 16,411–16,432, 1998.

Sandholm, S. T., et al., Summertime tropospheric observations related to N$_x$O$_y$ distributions and partitioning over Alaska: ABLE 3A, *J. Geophys. Res.*, *97*, 16,481–16,509, 1992.

Sandholm, S. T., et al., Summertime partitioning and budget of NO$_y$ compounds in the troposphere over Alaska and Canada: ABLE-3B, *J. Geophys. Res.*, *99*, 1837–1861, 1994.

Sandu, A., J. G. Verwer, M. Van Loon, G. R. Carmichael, F. A. Potra, D. Dabdub, and J. H. Seinfeld, Benchmarking stiff ODE solvers for atmospheric chemistry problems: I. Implicit vs explicit, *Atmos. Environ.*, *31*, 3151–3166, 1997.

Smyth, S., et al., Comparison of western Pacific air mass classification schemes for the PEM-West A experiment, *J. Geophys. Res.*, *101*, 1743–1762, 1996.

Streets, D. G., S. K. Guttikunda, and G. R. Carmichael, The growing contribution of sulfur emissions from ships in Asian waters, 1988–1995, *Atmos Environ*, *34*, 4425–4439, 2000.

Streets, D., et al., An inventory of gaseous and primary aerosol emissions in Asia in the year 2000, *J. Geophys. Res*, *108*(D21), 8809, doi:10.1029/2002JD003093, in press, 2003.

Thornhill, K. L., B. E. Anderson, J. D. Barrick, D. Bagwell, R. Friesen, and D. H. Lenschow, Air motion intercomparison flights during TRACE-P/ACE-Asia, *J. Geophys. Res.*, *108*(D20), 8783, doi:10.1029/2002JD003108, in press, 2003.

Thornton, D. C., A. R. Bandy, B. W. Blomquist, D. D. Davis, and R. W. Talbot, Sulfur dioxide as a source of condensation nuclei in the upper troposphere of the Pacific Ocean, *J. Geophys. Res.*, *101*, 1883–1890, 1996.

Thornton, D. C., A. R. Bandy, B. W. Blomquist, R. W. Talbot, and J. E. Dibb, Transport of sulfur dioxide from the Asian Pacific Rim to the North Pacific troposphere, *J. Geophys. Res.*, *102*, 28,489–28,499, 1997.

Thornton, D. C., A. R. Bandy, B. W. Blomquist, A. R. Driedger, and T. P. Wade, Sulfur dioxide distribution over the Pacific Ocean, 1991–1996, *J. Geophys. Res.*, *104*, 5845–5854, 1999.

Thornton, D. C., A. R. Bandy, F. H. Tu, B. W. Blomquist, G. M. Mitchell, W. Nadler, and D. H. Lenschow, Fast airborne sulfur dioxide measurements by atmospheric pressure ionization mass spectrometry (APIMS), *J. Geophys. Res.*, *107*(D22), 4632, doi:10.1029/2002JD002289, 2002a.

Thornton, D. C., F. H. Tu, A. R. Bandy, M. Kim, L. Thornhill, J. D. Barrick, and B. Anderson, Dynamics of sulfur dioxide in the marine boundary during TRACE-P, *Eos AGU Trans.*, *83*(47), Fall Meet. Suppl., Abstract A62A-0120, 2002b.

Uno, I., et al., Regional chemical weather forecasting system CFORS: Model descriptions and analysis of surface observations at Japanese island stations during the ACE-Asia experiment, *J. Geophys.*, *108*, doi:10.1029/2002JD002845, in press, 2003.

Wang, Q., et al., Characteristics of the marine boundary layers during two Lagrangian measurement periods: 2. Turbulence structure, *J. Geophys. Res.*, *104*, 21,767–21,784, 1999.

————————————
A. R. Bandy, M.-S. Kim, D. C. Thornton, and F. H. Tu, Department of Chemistry, Drexel University, Philadelphia, PA 19104, USA. (alan.bandy@drexel.edu; thorntdc@drexel.edu; fhtu@drexel.edu)

G. Carmichael and Y. Tang, Center for Global and Regional Environmental Research, University of Iowa, 424 IATL, Iowa City, IA 52242, USA. (gcarmich@engineering.uiowa.edu; ytang@cgrer.uiowa.edu)

G. Sachse and L. Thornhill, NASA Langley Research Center, MS 483, Hampton, VA 23681, USA. (k.l.thornhill@larc.nasa.gov)
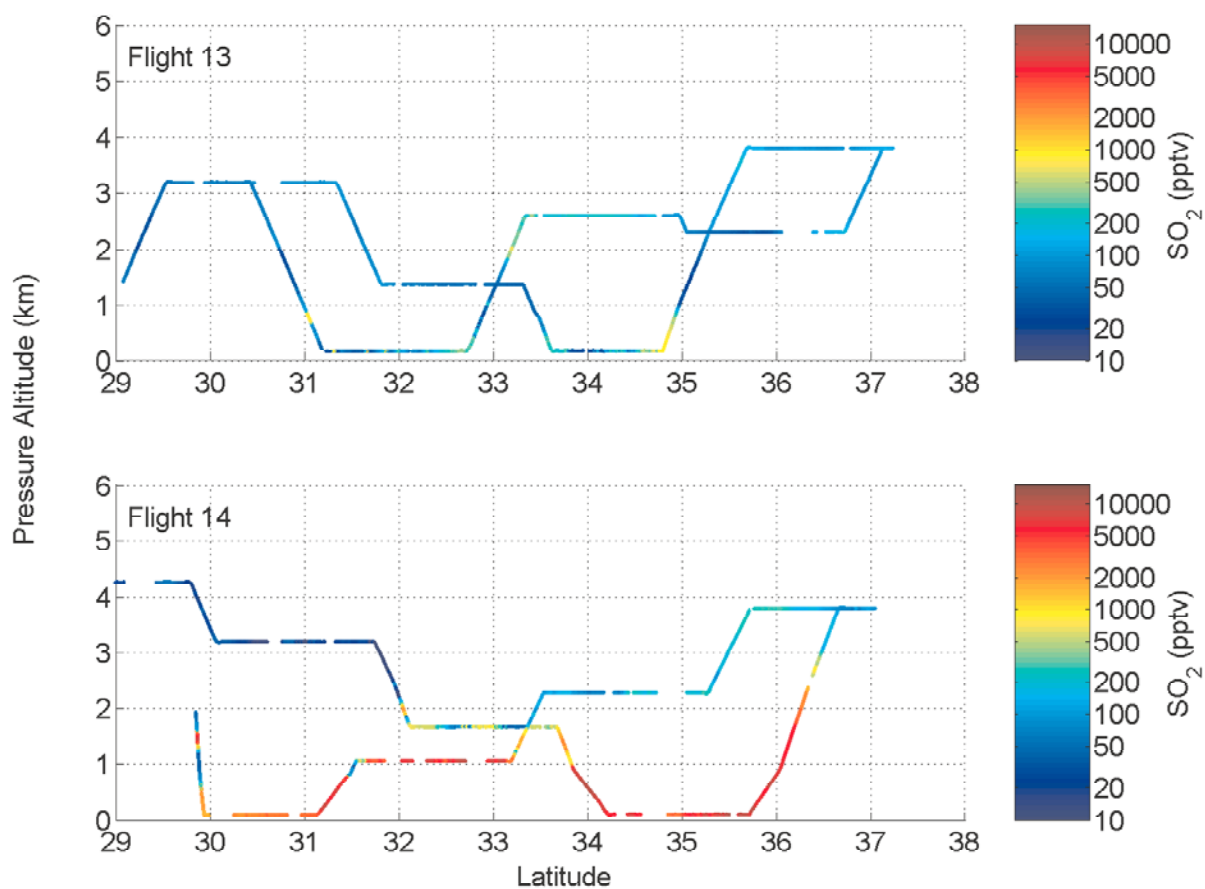
Figure 1. Sulfur dioxide distributions along the 124.5°E flight path for TRACE-P P-3B flight 13 during frontal passage and flight 14 behind the front. The profile just south of 30°N for flight 14 as the aircraft turned east from the 124.5°E track illustrates the downwind advection of SO₂.
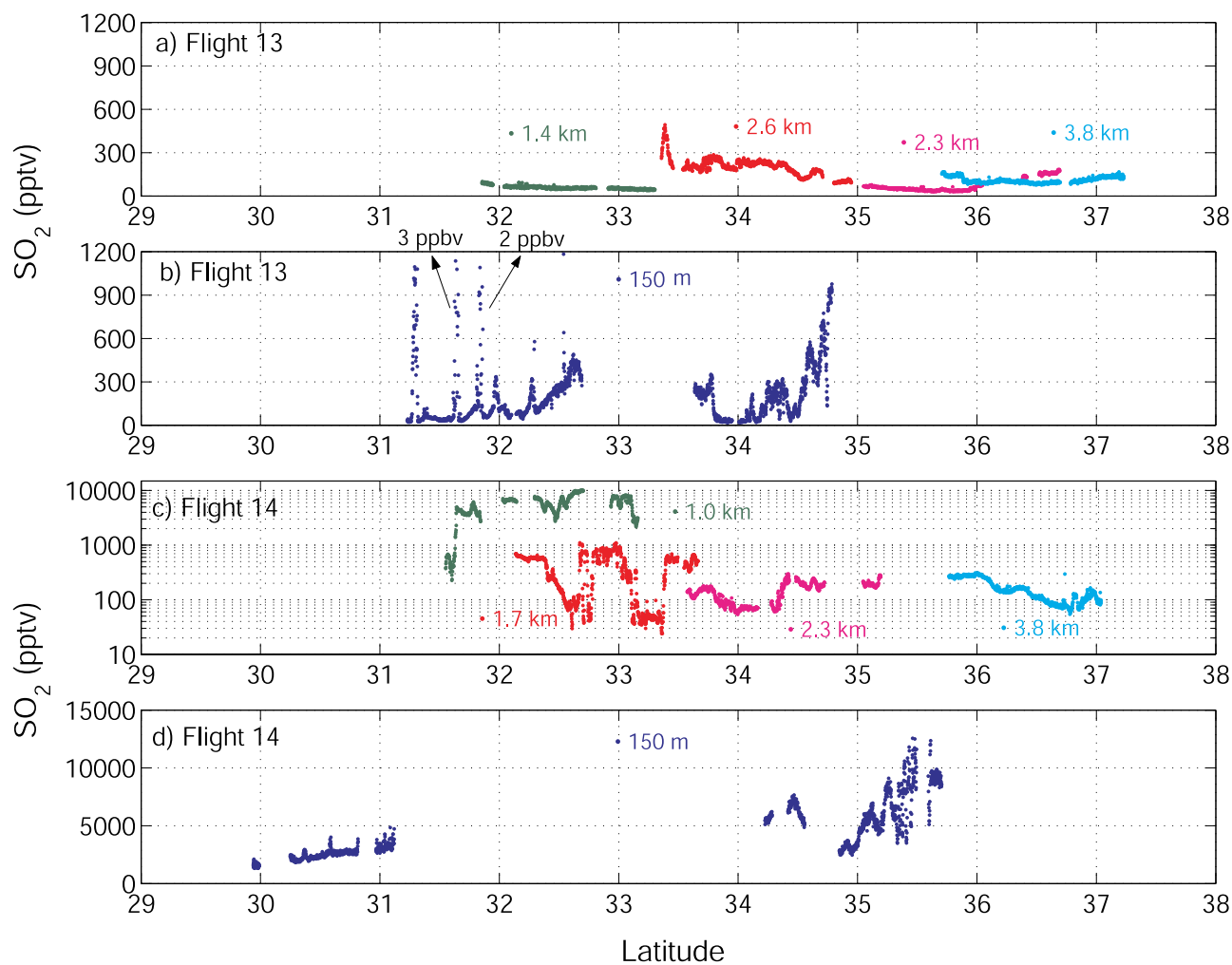
Figure 2. Sulfur dioxide distribution along 124.5°E for the level legs for flights 13 and 14. (a) and (c) above the mixed layer, (b) in mixed layer with spikes of SO$_2$ to 3 ppbv from ship plumes from 31.2°N to 32.5°N, (d) in the mixed layer for 30–31°N and in and out of the mixed layer between 34°N and 36°N.